

Performance Analysis of Integrated Sensing and Communications Under Gain-Phase Imperfections

Shuaishuai Han, *Student Member, IEEE*, Mohammad Ahmad Al-Jarrah, *Member, IEEE*,
Emad Alsusa, *Senior Member, IEEE*

Abstract

This paper evaluates the performance of uplink integrated sensing and communication systems in the presence of gain and phase imperfections. Specifically, we consider multiple unmanned aerial vehicles (UAVs) transmitting data to a multiple-input-multiple-output base-station (BS) that is responsible for estimating the transmitted information in addition to localising the transmitting UAVs. The signal processing at the BS is divided into two consecutive stages: localisation and communication. A maximum likelihood (ML) algorithm is introduced for the localisation stage to jointly estimate the azimuth-elevation angles and Doppler frequency of the UAVs under gain-phase defects, which are then compared to the estimation of signal parameters via rotational invariance techniques (ESPRIT) and multiple signal classification (MUSIC). Furthermore, the Cramer-Rao lower bound (CRLB) is derived to evaluate the asymptotic performance and quantify the influence of the gain-phase imperfections which are modelled using Rician and von Mises distributions, respectively. Thereafter, in the communication stage, the location parameters estimated in the first stage are employed to estimate the communication channels which are fed into a maximum ratio combiner to preprocess the received communication signal. An accurate closed-form approximation of the achievable average sum data rate (SDR) for all UAVs is derived. The obtained results show that gain-phase imperfections have a significant influence on both localisation and communication, however, the proposed ML is less sensitive when compared to other algorithms. The derived analysis is concurred with simulations.

The work of M. Al-Jarrah and E. Alsusa has received funding from the European Union's Horizon 2020 under grant agreement No 812991.

Shuaishuai Han, M. A. Al-Jarrah, and E. Alsusa are with the Department of Electrical and Electronic Engineering, University of Manchester, Manchester M13 9PL, U.K. (e-mail: shuaishuai.han@postgrad.manchester.ac.uk, {mohammad.al-jarrah, e.alsusa}@manchester.ac.uk).

Index Terms

Cramer-Rao lower bound (CRLB), integrated sensing and communication (ISAC), maximum likelihood, maximum ratio combining (MRC)

I. INTRODUCTION

As a candidate technique for next-generation wireless communication systems, integrated sensing and communication (ISAC) has attracted widespread interest in distinct fields, such as massive connectivity for internet-of-things (IoT) devices, unmanned aerial vehicles (UAVs), etc. [1], [2]. In the past decades, radar sensing [3] and communication research [4], [5] used to be conducted in parallel using different frequency bands. However, this traditionally separated design underutilizes system resources. Compared to the separated sensing and communication systems, ISAC allows both systems to share the same network resources and hardware appliances. Moreover, some important scenarios including autonomous driving and Wi-Fi sensing need reliable communications in addition to high-precision sensing, which increases the demands on ISAC systems.

Multiple-input-multiple-output (MIMO) is an advanced radar technology, which employs multiple antennas to generate multiple beams and receive multiple reflected signals from targets to improve radar performance [6]. On the other hand, conventional phased-array radars utilise multiple antennas to steer a beam towards a certain target. As such, MIMO radars provide superior performance compared to phased-array radars for ISAC. Consequently, this paper is interested in studying a MIMO radar with a uniform rectangular array

(URA) to receive data signals from multiple drones and use these signals to localise the drones in addition to decoding the information contents.

To boost communication and sensing performance, high-performance localisation algorithms and efficient communication signal pre-processing techniques are indispensable. Efficient localisation algorithms include the estimation of signal parameters via rotational invariance techniques (ESPRIT), multiple signal classification (MUSIC) and maximum likelihood (ML) algorithms. Both ESPRIT and MUSIC are parameter estimation algorithms, where the former accurately estimates the location parameters of multiple sources by leveraging the rotational invariance property of the covariance matrix [7], whilst the latter estimates multiple signals amidst noise by using signal and noise subspaces [8]. Compared to ESPRIT and MUSIC, the maximum likelihood algorithm provides the optimal localisation performance, as shown in [9]. On the other hand, signal pre-processing methods for communication signals include, but are not limited to, maximum ratio combining (MRC) [10], which optimally combines received signals from multiple receiving antennas according to their respective signal strengths to enhance signal quality and communication reliability.

A. Literature Review

In recent years, much research has been conducted towards achieving higher communication and localisation performance using the same platform. In [11], a field test on the feasibility of joint communication and radar imaging is conducted using an airborne MIMO radar. The experimental results demonstrated that data transmission and high-resolution radar sensing can be performed at the same time without intramodal

interference. Optimal waveform design and the orthogonal time frequency space (OTFS) transmission for ISAC systems were investigated in [12] and [13]. In [14], the performance of both downlink and uplink ISAC systems is analysed. The results showed that ISAC can offer more degrees of freedom for both communication rate (CR) and sensing rate (SR) than traditional frequency-division sensing and communication (FDSAC) systems where isolated frequency bands are utilised for sensing and communication. In addition, the superiority of ISAC over FDSAC was also demonstrated in [15], where CR and SR are utilised to evaluate the communication and sensing performance of the ISAC system, respectively. In [16], [17], the authors propose a performance framework based on Kullback-Leibler divergence (KLD) for ISAC systems to unify the evaluation measure for both subsystems. In contrast to the evaluation measures used in [14]-[17], in [18] and [19] the achievable root mean square error (RMSE) and sum data rate (SDR) are employed separately to evaluate the performance of ISAC systems.

Albeit, neither the communication performance nor the positioning performance of the above ISAC systems can be guaranteed in real-life applications where array model errors, such as gain and phase defects, exist. Gain and phase defects arise as the gain and phase of the antenna may differ from their state after the previous calibration. This can be caused by the gradual changes in the behaviour of the individual antenna and of the electronic circuitry between the antenna and the digitizer output due to ageing of components, thermal effects, etc [20]-[22]. Gain-phase defects are very critical and will cause erroneous localisation and communication degradation of the ISAC system if they are overlooked. Hence, some calibration approaches

have been developed to eliminate array model errors including gain-phase defects [23], [24]. However, even when the initial calibration is perfect, regular calibration is required as the system characteristics vary over time when the surrounding environment changes, which makes it very challenging to completely solve the array model defects issue in practical applications.

Much efforts have been devoted in the past decade to quantify the effect of array model defects on antenna systems. In [25], the authors provide performance evaluation and the Cramer–Rao bound (CRB) of the coarray-based MUSIC algorithm under the effect of small sensor location errors with real Gaussian distribution. Their results indicate that sensor position defects introduce a constant bias, which cannot be eradicated by only increasing the signal-to-noise ratio (SNR). In [26], [27], CRB conditioned on gain-phase errors with real Gaussian distribution is derived. However, this conditional CRB cannot capture the actual behaviour of gain-phase errors as the errors vary over time in real-world scenarios. In [28], [29], the uniform distribution is employed to model both the gain and phase defects. However, the aforementioned works in [25]-[29] have considered MIMO radar systems only rather than ISAC, and used oversimplified errors models that do not capture the characteristics of the errors.

B. Motivation and Contributions

It can be seen from the above surveyed literature that there is a need for further investigations on the operation of ISAC systems under model imperfections, and that the design of simple and effective tools for localisation under such conditions is indispensable. Motivated by these facts, this paper investigates the

impact of gain-phase errors on the functionality of ISAC systems, where in contrast to [25]-[29], a general error model is applied. More specifically, Rician and von Mises random processes are used to model the gain and phase errors, respectively. Also, the system model considered consists of multiple drones communicating with a MIMO base station (MIMO-BS) equipped with a URA which is responsible for decoding information and localising the drones by utilising pilot signals inserted in the information packets. The entire process at MIMO-BS is divided into two stages, where the localisation process is performed in the first stage to jointly estimate the azimuth angle, elevation angle and Doppler frequency of the drones. Thereafter, in the second stage, the estimated parameters are used to estimate the channel response and then MRC is applied to estimate the transmitted information. Intuitively, the gain-phase errors will cause some estimation errors in the first stage, which affects the decoding process of the transmitted information in the second stage. To the best of our knowledge, no previous work has considered the effect of gain-phase defects on ISAC systems. Hence, the main contributions of this paper can be summarized as follows.

- 1) A practical and efficient system model for uplink ISAC systems consisting of MIMO-BS and multiple UAVs is introduced and investigated for scenarios where GPS signals are poor and precise location information is infeasible. To achieve both communication and localisation at the MIMO-BS, two possible scenarios are considered, where signal processing is divided into localisation and communication stages. Rician and von Mises distributions are invoked to provide generalised models for gain and phase imperfections, respectively.

- 2) A maximum likelihood estimator (MLE) and a novel alternating optimisation based maximum likelihood (AO-ML) algorithm are derived for location parameters under the effect of gain-phase defects. In addition, a closed-form expression for the average CRLB of the proposed MLE is obtained to evaluate the performance limits of the localisation subsystem. To the best of our knowledge, no previous work has considered MLE and the average CRLB in the case of MIMO-BS under model errors. Moreover, the achievable RMSE is compared with other widely used alternatives including MUSIC and ESPRIT.
- 3) A novel approach for decoding information from the received signals is proposed for the communication stage. The decoding process includes the utilisation of the estimated location parameters by various localisation algorithms to infer the channel responses. The estimated channel responses are employed to combine signals using MRC in order to preprocess the received communication signal vector and improve the received signal quality. It is also found that the location parameters estimated by different algorithms with gain-phase defects follow Gaussian distributions with equal mean values, which are the actual location parameters, but different variances.
- 4) Because the exact solution for the achievable sum rate is not tractable, an accurate approximation for the average data rate of the preprocessed signal is derived under the aforementioned system imperfections. According to the closed-form expressions of the average data rate, the estimation errors of Doppler frequency by the localisation algorithms do not influence the average data rate.
- 5) Simulation results for the RMSE of various localisation algorithms and the average sum data rate are

provided for two scenarios under gain-phase errors conditions. It is shown that these results match well with the theoretical analysis and show that both the RMSE and average sum data rate are degraded by gain-phase defects, especially ESPRIT, which completely fails in some cases.

The remainder of this paper is organised as follows. In Sec. II, the system model for the ISAC scenario of interest is presented. Sec. III shows the proposed maximum likelihood algorithms and CRLB, whilst Sec. IV provides the uplink communication with MRC and the proposed approximation method. Sec. V provides the numerical results and Sec. VI concludes the paper.

Notations: $[\cdot]^T$ and $[\cdot]^H$ denote the transposition and Hermitian transposition of a matrix, respectively. $[\cdot]^*$ represents the conjugate of a complex value. $\|\cdot\|_2$ refers to the Euclidean norm. $\text{var}(\cdot)$ and $\text{cov}(\cdot)$ denote the variance and covariance, respectively. $\text{tr}(\cdot)$ stands for the trace of a square matrix, and $\Re(\cdot)$ indicates the real part of an input argument. $\mathbb{E}[\cdot]$ indicates the statistical expectation. $\Gamma(\cdot)$ represents the Gamma function.

II. SYSTEM MODEL

This work considers an uplink ISAC system, where a number of K mobile single-antenna drones, each of which has a Doppler frequency of $f_{D,k}$ Hz for any $k = \{1, \dots, K\}$ in the far field, are employed to send information signals to a MIMO-BS. The model is applicable to GPS-denied environments, for example, suburbs [30] or adversary-controlled airspace [31], where precise drone localisation is infeasible. In this case, information signals can be sent actively by drones to the MIMO-BS, where it is assumed that only the Line-of-Sight (LOS) channel is considered. Once these signals are received by the MIMO-BS, it will process the

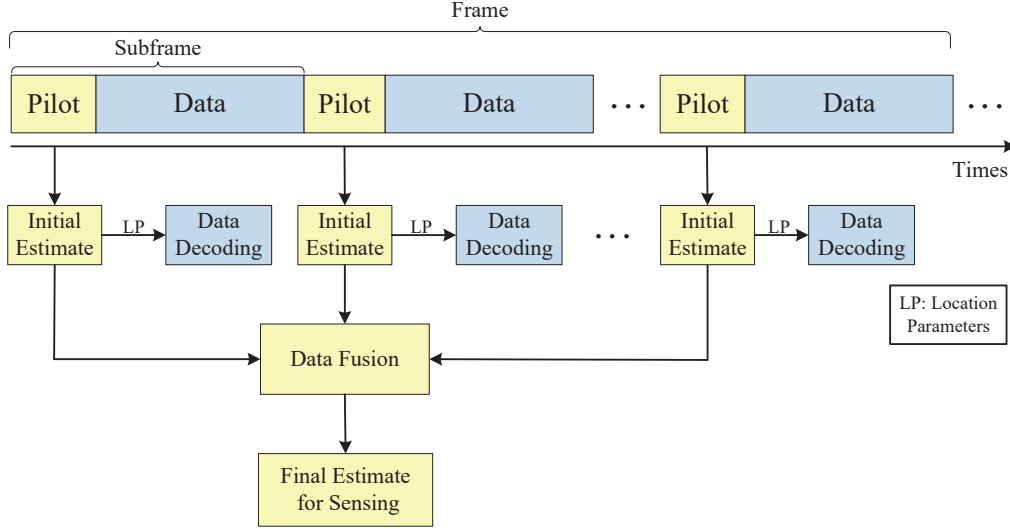


Fig. 1. Frame structure of the ISAC system.

signals and obtain both the location, i.e., the azimuth angle, elevation angle and Doppler frequency, of the drones and the transmitted symbols. The MIMO-BS is composed of a URA with $M \times N$ antennas, where M and N denote the number of antennas along the x -axis and y -axis, respectively. The distance between two adjacent antennas along the x -axis is denoted by d_x , while it is represented along the y -axis by d_y . Without loss of generality, $d_x = d_y = d = \lambda/2$, where λ denotes the signal wavelength. The azimuth angle and elevation angle of the signal received by the MIMO-BS from the k th drone can be represented as ϕ_k and θ_k , respectively. In addition, we assume that all antennas in the MIMO-BS suffer from gain-phase defects and non-coherent estimation [32] is adopted in the ISAC system.

In order to estimate the azimuth-elevation-Doppler frequency and decode the transmitted symbols at the MIMO-BS, the frame structure shown in Fig. 1 is considered, where each frame is composed of t_L subframes. Similar to the assumption on the frame structure in [33], we are targeting the scenario in which the velocities and positions of the drones are relatively stable during a frame period. As a consequence, the azimuth-

elevation angles and Doppler frequency are assumed to be time-invariant during the frame period as their changes can be regarded as negligible. For instance, 3.125×10^{-7} seconds are required to transmit a number of 10^4 symbols in each frame with a baud rate of 32 Gbaud [34], and thus the typical velocity of drones is much less than the transmission rate which makes the changes in their positions very small during the transmission of a frame.

In addition, two possible scenarios for data detection are considered in this paper. In scenario I, a pilot signal is employed to provide the initial estimates for the location parameters in each subframe, which will be used for decoding data symbols in that subframe. After estimating the parameters of t_L periods using t_L pilots, the final estimates for parameters, which are used to declare the localisation parameters, will be evaluated based on t_L snapshots, where one snapshot is selected at the pilot for each subframe. In this paper, this scenario is referred to Single Pilot based Decoding and Multiple Pilots based Localisation (SPD-MPL). On the other hand, in scenario II, the MIMO-BS adopts a number of t_L pilots for estimating location parameters and then decodes the transmitted symbols for all the t_L subframes by using the estimated location parameters. Throughout this paper, this scenario is referred to Multiple Pilots based Decoding and Multiple Pilots based Localisation (MPD-MPL). It is noteworthy to mention that MPD-MPL is expected to provide better achievable capacity as the estimated parameters used for data detection are more reliable, however, it would increase the system latency and require considerable memory and computational resources. Therefore, there is a trade-off between complexity and performance, and SPD-MPL could suit low-latency systems more.

After receiving the t_l th pilot signal from all drones by the MIMO-BS and then arranging the outputs of the matched filter, the received signal vector can be written as

$$\mathbf{y}(t_l) = \mathbf{A}\Phi\boldsymbol{\omega}(t_l) + \mathbf{n}(t_l), \quad (1)$$

where $\mathbf{A} \in \mathbb{C}^{MN \times K}$ denotes the array manifold of MIMO-BS and Φ refers to the diagonal matrix, which is defined as $\Phi \triangleq \text{diag}\{a_{t,1}s_{p,1}(t_l), \dots, a_{t,K}s_{p,K}(t_l)\}$, where $a_{t,k}$ represents the response of the k th single-antenna drone with $a_{t,k} = 1$ and $s_{p,k}(t_l)$ indicates the transmitted pilot signal with $s_{p,k}(t_l) = 1$, thus Φ is an identity matrix. The vector $\boldsymbol{\omega}(t_l)$ indicates the vector with $\boldsymbol{\omega}(t_l) \triangleq [\eta_1 e^{j2\pi f_{D,1}t_l/f_s}, \dots, \eta_K e^{j2\pi f_{D,K}t_l/f_s}]^T$ where f_s represents the signal sampling frequency, η_k includes the pass loss and complex reflection factor, which is proportional to the radar cross section (RCS) of the k th drone, and $\mathbf{n}(t_l)$ represents the noise vector consisting of additive white Gaussian noise (AWGN) samples. For convenience, the values of η_k are normalized to unity, i.e., $\eta_k = 1 \forall k$. The matrix \mathbf{A} can be expressed as $\mathbf{A} = [\mathbf{a}(\phi_1, \theta_1), \dots, \mathbf{a}(\phi_K, \theta_K)]$ [35], in which the steering vector of the URA towards the k th drone $\mathbf{a}(\phi_k, \theta_k)$ can be given by

$$\mathbf{a}(\phi_k, \theta_k) = [a_{1,1}(\phi_k, \theta_k), \dots, a_{M,N}(\phi_k, \theta_k)]^T, \quad (2)$$

where $a_{m,n}(\phi_k, \theta_k) \triangleq \alpha_{m,n} e^{j\Delta\delta_{m,n}} e^{-j2\pi\vartheta/\lambda} \quad \forall \{m, n\} \leq \{M, N\}$, where $\alpha_{m,n}$ and $\Delta\delta_{m,n}$ represent the gain defects and phase defects of the (m, n) th antenna, respectively, and ϑ can be denoted by $\vartheta = (m - 1)d \cos \phi_k \sin \theta_k + (n - 1)d \sin \phi_k \sin \theta_k$.

By utilising a number of t_L pilots during the whole frame, the received signal matrix \mathbf{Y} can be obtained as

$$\mathbf{Y} = \mathbf{A}\boldsymbol{\Omega} + \mathbf{N}, \quad (3)$$

where $\mathbf{Y} = [\mathbf{y}(t_1), \dots, \mathbf{y}(t_L)] \in \mathbb{C}^{MN \times t_L}$. $\boldsymbol{\Omega}$ denotes the Doppler frequency matrix, which is given by $\boldsymbol{\Omega} =$

$[\boldsymbol{\omega}(t_1), \dots, \boldsymbol{\omega}(t_L)]$ and \mathbf{N} denotes the AWGN matrix.

During each subframe, a number of Q symbols are transmitted from the corresponding drones to the MIMO-BS. As a consequence, we can obtain the received signal vector for each transmitted symbol, which can be denoted by

$$\bar{\mathbf{y}} = \mathbf{A}\mathbf{W}\mathbf{s} + \bar{\mathbf{n}}, \quad (4)$$

where $\bar{\mathbf{y}} \in \mathbb{C}^{MN \times 1}$, $\mathbf{A}\mathbf{W}$ denotes the equivalent channel response with $\mathbf{W} \triangleq \text{diag}(e^{j2\pi f_{D,1}/f_s}, \dots, e^{j2\pi f_{D,K}/f_s})$, \mathbf{s} represents the signal vector consisting of the transmitted symbols with $\mathbf{s} = [s_1, \dots, s_K]^T$, where s_k denotes the transmitted symbol from the k th drone and $\bar{\mathbf{n}}$ indicates the noise vector.

A. Gain-Phase Defects Model

To begin, let us define $h_{m,n} \triangleq \alpha_{m,n} e^{j\Delta\delta_{m,n}}$ to denote the gain-phase defects of the (m, n) th antenna, which are independent across different antennas. Interestingly, by employing this model, it can be observed that $h_{m,n}$ has a similar form to fading channels. Therefore, we assume $h_{m,n}$ follows the complex Gaussian distribution, i.e., $h_{m,n} \sim \mathcal{CN}(\mu_h, \sigma_h^2)$, which is a commonly used model in which μ_h represents the complex mean of $h_{m,n}$ and $\sigma_h^2 = 2\sigma_0^2$, where σ_0^2 indicates the variance of the real and imaginary parts of $h_{m,n}$. Accordingly, the amplitude of $h_{m,n}$ (i.e., gain imperfections) follows a Rician distribution [36], whereas the phase of $h_{m,n}$ (i.e., phase defects) follows a von Mises distribution. The probability density function (PDF) of the Rician distribution is denoted by

$$f(\alpha_{m,n}) = \frac{\alpha_{m,n}}{\sigma_r^2} e^{-\frac{(\alpha_{m,n}^2 + \nu^2)}{2\sigma_r^2}} I_0\left(\frac{\alpha_{m,n}\nu}{\sigma_r^2}\right), \quad (5)$$

where ν and σ_r represent the location and scale parameters of the Rician distribution, respectively and $I_0(x)$ is the modified Bessel function of the first kind with zero order. In general, the modified Bessel function of the first kind with an order of q can be defined as the following infinite series.

$$I_q(x) = \sum_{b=0}^{\infty} \frac{1}{b! \Gamma(b+q+1)} \left(\frac{x}{2}\right)^{2b+q}. \quad (6)$$

As phase errors follow the independent von Mises distribution, the PDF can be denoted by

$$f(\Delta\delta_{m,n}) = \frac{1}{2\pi I_0(\tilde{k})} e^{\tilde{k} \cos(\Delta\delta_{m,n} - \tilde{\mu})}, \quad (7)$$

where $\tilde{\mu}$ and \tilde{k} denote the measures of location and concentration, respectively. The probability density can be also denoted by using a series of Bessel functions as

$$f(\Delta\delta_{m,n}) = \frac{1}{2\pi} \left(1 + \frac{2}{I_0(\tilde{k})} \sum_{q=1}^{\infty} I_q(\tilde{k}) \cos[q(\Delta\delta_{m,n} - \tilde{\mu})] \right). \quad (8)$$

Since the ideal case of phase defects is zero (e.g. $\Delta\delta_{m,n} = 0$), the mean value of the phase error is typically $\tilde{\mu} = 0$. Therefore, the phase defects are distributed around 0 with a density function characterized by the value \tilde{k} only. When \tilde{k} increases, as the shape of the von Mises distribution becomes sharper, the values of phase imperfections will be more concentrated around $\tilde{\mu} = 0$.

III. STAGE I: MAXIMUM LIKELIHOOD ESTIMATION AND CRLB

A. Maximum Likelihood Estimation

First of all, by vectorising \mathbf{Y} in (3), the received signal vector $\tilde{\mathbf{y}}$ can be obtained as

$$\tilde{\mathbf{y}} = \left\{ \left\{ \mathbf{A}\boldsymbol{\omega}(t_1) \right\}^T, \dots, \left\{ \mathbf{A}\boldsymbol{\omega}(t_L) \right\}^T \right\}^T + \tilde{\mathbf{n}}, \quad (9)$$

where $\tilde{\mathbf{y}} \in \mathbb{C}^{MNt_L \times 1}$. The variables in $\tilde{\mathbf{y}}$ include gain-phase defects in \mathbf{A} and AWGN noise. Given that both of them follow the complex Gaussian distribution, $\tilde{\mathbf{y}}$ also follows a complex Gaussian distribution. The PDF of $\tilde{\mathbf{y}}$ conditioned on $\boldsymbol{\gamma}$ can be denoted by [37]

$$f(\tilde{\mathbf{y}}|\boldsymbol{\gamma}) = 1/(\pi^{MNt_L} \det(\boldsymbol{\Gamma})) e^{-[\tilde{\mathbf{y}}-\boldsymbol{\mu}]^H \boldsymbol{\Gamma}^{-1}[\tilde{\mathbf{y}}-\boldsymbol{\mu}]}, \quad (10)$$

where $\boldsymbol{\gamma} = [\boldsymbol{\phi}^T, \boldsymbol{\theta}^T, \mathbf{f}_D^T]^T$, which refers to the vector consisting of the deterministic unknown location parameters, where $\boldsymbol{\phi} = [\phi_1, \dots, \phi_K]$, $\boldsymbol{\theta} = [\theta_1, \dots, \theta_K]$ and $\mathbf{f}_D = [f_{D,1}, \dots, f_{D,K}]$. The covariance matrix $\boldsymbol{\Gamma}$ and mean vector $\boldsymbol{\mu}$ can be respectively given by $\boldsymbol{\Gamma} = \mathbb{E}[(\tilde{\mathbf{y}} - \boldsymbol{\mu})(\tilde{\mathbf{y}} - \boldsymbol{\mu})^H]$ and

$$\boldsymbol{\mu} = \left\{ \left\{ \mathbb{E}[\mathbf{A}\boldsymbol{\omega}(t_1)] \right\}^T, \dots, \left\{ \mathbb{E}[\mathbf{A}\boldsymbol{\omega}(t_L)] \right\}^T \right\}^T, \quad (11)$$

where the mnt_L th elements in $\boldsymbol{\mu}$ can be expressed by

$$\boldsymbol{\mu}(mnt_L) = \sum_{k=1}^K \left\{ \mathbb{E}[\alpha_{m,n}] \mathbb{E}[e^{j\Delta\delta_{m,n}}] e^{-j2\pi\vartheta/\lambda} e^{j2\pi f_{D,k} t_1 / f_s} \right\}, \quad (12)$$

where the closed-form expressions of $\mathbb{E}[\alpha_{m,n}]$ and $\mathbb{E}[e^{j\Delta\delta_{m,n}}]$ can be obtained by using Theorem 1 and the derivation in Appendix A, respectively.

The (i, j) th element in $\boldsymbol{\Gamma}$, where $i, j = \{1, \dots, MNt_L\}$, can be denoted by

$$\boldsymbol{\Gamma}_{i,j} = \mathbb{E}[\alpha_u \alpha_v] \mathbb{E}[e^{j\Delta\delta_u - j\Delta\delta_v}] Q_i Q_j^* - \mathbb{E}[\alpha_u] \mathbb{E}[e^{j\Delta\delta_u}] \mathbb{E}[\boldsymbol{\mu}(j)]^* Q_i - \mathbb{E}[\alpha_v] \mathbb{E}[e^{-j\Delta\delta_v}] \mathbb{E}[\boldsymbol{\mu}(i)] Q_j^* + \mathbb{E}[\boldsymbol{\mu}(i)] \mathbb{E}[\boldsymbol{\mu}(j)]^*, \quad (13)$$

where (α_u, α_v) and (δ_u, δ_v) denote the gain and phase defects in the (i, j) th element of $\boldsymbol{\Gamma}$, where $u, v = \{1, \dots, MN\}$. Q_i and Q_j can be given by using their general expression Q_o for $o \in \{i, j\}$, which is given by

$$Q_o = \sum_{k=1}^K \left\{ e^{-j2\pi\vartheta_o/\lambda} e^{j2\pi f_{D,k} t_{1o} / f_s} \right\}, \quad (14)$$

where $\vartheta_o = (m_o - 1)d \cos \phi_k \sin \theta_k + (n_o - 1)d \sin \phi_k \sin \theta_k$, where $m_o \in \{1, \dots, M\}$ and $N_o \in \{1, \dots, N\}$.

In (13), $\mathbb{E}[\alpha_u \alpha_v] = \mathbb{E}[\alpha_u^2]$, where the closed-form expressions of $\mathbb{E}[\alpha_u^2]$ can be obtained by using Theorem 1 and $\mathbb{E}[e^{j\Delta\delta_u - j\Delta\delta_v}] = 1$ if $u = v$. However, $\mathbb{E}[\alpha_u \alpha_v] = \mathbb{E}[\alpha_u] \mathbb{E}[\alpha_v]$ and $\mathbb{E}[e^{j\Delta\delta_u - j\Delta\delta_v}] = \mathbb{E}[e^{j\Delta\delta_u}] \mathbb{E}[e^{-j\Delta\delta_v}]$ if $u \neq v$, where the closed-form expressions of $\mathbb{E}[\alpha_u]$ and $\mathbb{E}[\alpha_v]$ can also be obtained by using Theorem 1. In addition, the closed-form expressions of $\mathbb{E}[e^{j\Delta\delta_u}]$ and $\mathbb{E}[e^{-j\Delta\delta_v}]$ can be obtained

by using the derivations of their general expression $\mathbb{E}[e^{\pm jC\Delta\delta_a}]$ in Appendix A, where C denotes a constant value.

Eventually, the maximum likelihood estimator (MLE), which can identify the parameter values that optimise the log-likelihood function over the parameter space, can be given by

$$[\boldsymbol{\phi}, \boldsymbol{\theta}, \mathbf{f}_D] = \arg \max_{\boldsymbol{\phi}, \boldsymbol{\theta}, \mathbf{f}_D} \ln f(\tilde{\mathbf{y}}|\boldsymbol{\gamma}), \quad (15)$$

By removing constant terms which do not impact the maximization operation, (15) can be simplified to

$$\begin{aligned} [\boldsymbol{\phi}, \boldsymbol{\theta}, \mathbf{f}_D] &= \arg \min_{\boldsymbol{\phi}, \boldsymbol{\theta}, \mathbf{f}_D} (\tilde{\mathbf{y}} - \boldsymbol{\mu})^H \boldsymbol{\Gamma}_n^{-1} (\tilde{\mathbf{y}} - \boldsymbol{\mu}) \\ &= \arg \min_{\boldsymbol{\phi}, \boldsymbol{\theta}, \mathbf{f}_D} \|\tilde{\mathbf{y}} - \boldsymbol{\mu}\|_2^2. \end{aligned} \quad (16)$$

B. The AO-ML Algorithm

Due to the high computational complexity of the ML algorithm, we propose a low complexity AO-ML algorithm. It uses an alternating optimization method, where the maximum likelihood algorithm is adopted to optimize one or two variables while keeping the other variables fixed in each iteration. By using the PDF of $\tilde{\mathbf{y}}$ in (10) and following steps similar to (15) and (16), the first phase of the l th iteration of AO-ML includes estimating $\mathbf{f}_D^{(l)}$ given $\boldsymbol{\phi}^{(l-1)}$ and $\boldsymbol{\theta}^{(l-1)}$, where l indicates the l th iteration, can be expressed as

$$\left[\mathbf{f}_D^{(l)} \right] = \arg \min_{\mathbf{f}_D^{(l)}} \left\| \tilde{\mathbf{y}} - \left\{ \left\{ \mathbb{E}[\mathbf{A}(\boldsymbol{\phi}^{(l-1)}, \boldsymbol{\theta}^{(l-1)})\boldsymbol{\omega}(t_1)] \right\}^T, \dots, \left\{ \mathbb{E}[\mathbf{A}(\boldsymbol{\phi}^{(l-1)}, \boldsymbol{\theta}^{(l-1)})\boldsymbol{\omega}(t_L)] \right\}^T \right\}^T \right\|_2^2, \quad (17)$$

where $\boldsymbol{\phi}^{(0)}$ and $\boldsymbol{\theta}^{(0)}$ indicate the initial values for azimuth angle and elevation angle in the AO-ML algorithm when $l = 1$.

In the second phase, the MLE for $\boldsymbol{\phi}^{(l)}$ and $\boldsymbol{\theta}^{(l)}$ given $\mathbf{f}_D^{(l-1)}$ can be given by

$$\left[\boldsymbol{\phi}^{(l)}, \boldsymbol{\theta}^{(l)} \right] = \arg \min_{\boldsymbol{\phi}^{(l)}, \boldsymbol{\theta}^{(l)}} \left\| \tilde{\mathbf{y}} - \left\{ \left\{ \mathbb{E}[\mathbf{A}\boldsymbol{\omega}(\mathbf{f}_D^{(l-1)}, t_1)] \right\}^T, \dots, \left\{ \mathbb{E}[\mathbf{A}\boldsymbol{\omega}(\mathbf{f}_D^{(l-1)}, t_L)] \right\}^T \right\}^T \right\|_2^2, \quad (18)$$

where $\mathbf{f}_D^{(0)}$ refers to the initial value for Doppler frequency. Afterwards, the input $\phi^{(l-1)}$ and $\theta^{(l-1)}$ of (17) and the input $\mathbf{f}_D^{(l-1)}$ of (18) will be updated after each iteration until the AO-ML algorithm converges. The convergence of the AO-ML algorithm can be determined by the following criterion:

$$\|\gamma^{(l)} - \gamma^{(l-1)}\|_2 < \epsilon, \quad (19)$$

where $\gamma^{(l)} \in \{\phi^{(l)}, \theta^{(l)}, \mathbf{f}_D^{(l)}\}$ and then the outputs of (17) and (18) are the solutions obtained by using the AO-ML algorithm once convergence is reached.

C. The Genie Maximum Likelihood Estimation

In order to provide a benchmark for the ML and AO-ML algorithms, a genie maximum likelihood (G-ML) estimation is derived by assuming that the amount of gain-phase defects has been perfectly estimated by the auto-calibrated methods proposed in [24]. The plausibility of the assumption can be demonstrated by using the results in [38], which shows that the average bias of the estimated gain and phase defects compared to their actual values are very small. By using this assumption, gain and phase defects are known in the G-ML estimation and thus we can obtain the PDF of $\tilde{\mathbf{y}}$ conditioned on $\hat{\boldsymbol{\gamma}}$, where $\hat{\boldsymbol{\gamma}}$ denotes the vector consisting of the unknown location parameters and gain-phase defects. $\tilde{\mathbf{y}}$ can be written as

$$f(\tilde{\mathbf{y}}|\hat{\boldsymbol{\gamma}}) = 1/\left(\pi^{MNt_L} \det(\hat{\mathbf{\Gamma}})\right) e^{-[\tilde{\mathbf{y}}-\hat{\boldsymbol{\mu}}]^H \hat{\mathbf{\Gamma}}^{-1} [\tilde{\mathbf{y}}-\hat{\boldsymbol{\mu}}]}, \quad (20)$$

where $\hat{\mathbf{\Gamma}}$ indicates the noise covariance matrix, and $\hat{\boldsymbol{\mu}}$ is

$$\hat{\boldsymbol{\mu}} = \left\{ \left\{ \mathbf{A}\boldsymbol{\omega}(t_1) \right\}^T, \dots, \left\{ \mathbf{A}\boldsymbol{\omega}(t_L) \right\}^T \right\}^T. \quad (21)$$

By following steps similar to (15) and (16) again, the MLE of the G-ML estimation can be obtained, which is denoted by

$$[\boldsymbol{\phi}, \boldsymbol{\theta}, \mathbf{f}_D] = \arg \min_{\boldsymbol{\phi}, \boldsymbol{\theta}, \mathbf{f}_D} \|\tilde{\mathbf{y}} - \hat{\boldsymbol{\mu}}\|_2^2. \quad (22)$$

D. Cramer–Rao Lower Bound (CRLB)

Based on the proposed ML algorithm in Sec. III. A, the CRLB for the azimuth-elevation-Doppler estimation is derived in this section as a benchmark for the localisation performance of the considered ISAC system. In order to obtain the CRLB, a Fisher information matrix (FIM) is derived first, which is defined as

$$\mathbf{F} \triangleq -\mathbb{E} \left[\partial^2 \ln f(\tilde{\mathbf{y}}|\boldsymbol{\gamma}) / \partial \boldsymbol{\gamma} \partial \boldsymbol{\gamma}^T \right], \quad (23)$$

where $\mathbf{F} \in \mathbb{C}^{3K \times 3K}$ and $\partial f(\tilde{\mathbf{y}}|\boldsymbol{\gamma}) / \partial \boldsymbol{\gamma}$ indicates the partial derivative of $f(\tilde{\mathbf{y}}|\boldsymbol{\gamma})$ with respect to $\boldsymbol{\gamma}$. As a consequence, the (i, j) th submatrix of \mathbf{F} is written as follows.

$$\mathbf{F}_{i,j} \triangleq -\mathbb{E} \left[\partial^2 \ln f(\tilde{\mathbf{y}}|\boldsymbol{\gamma}) / \partial \boldsymbol{\gamma}_i \partial \boldsymbol{\gamma}_j \right], \quad (24)$$

where $\mathbf{F}_{i,j} \in \mathbb{C}^{3 \times 3}$. According to the Slepian-Bangs formula [39, pp.363], which is specially designed for the Gaussian case, $\mathbf{F}_{i,j}$ can also be evaluated by

$$\mathbf{F}_{i,j} = \text{tr} \left[\boldsymbol{\Gamma}^{-1} \frac{\partial \boldsymbol{\Gamma}}{\partial \boldsymbol{\gamma}_i} \boldsymbol{\Gamma}^{-1} \frac{\partial \boldsymbol{\Gamma}}{\partial \boldsymbol{\gamma}_j} \right] + 2\Re \left[\frac{\partial \boldsymbol{\mu}^H}{\partial \boldsymbol{\gamma}_i} \boldsymbol{\Gamma}^{-1} \frac{\partial \boldsymbol{\mu}}{\partial \boldsymbol{\gamma}_j} \right]. \quad (25)$$

Since $\partial \boldsymbol{\Gamma} / \partial \boldsymbol{\gamma}_i = \partial \boldsymbol{\Gamma} / \partial \boldsymbol{\gamma}_j = 0$, $\mathbf{F}_{i,j}$ reduces to

$$\mathbf{F}_{i,j} = 2\Re \left[\frac{\partial \boldsymbol{\mu}^H}{\partial \boldsymbol{\gamma}_i} \boldsymbol{\Gamma}_n^{-1} \frac{\partial \boldsymbol{\mu}}{\partial \boldsymbol{\gamma}_j} \right], \quad (26)$$

where $\boldsymbol{\gamma}_i = [\boldsymbol{\phi}(i), \boldsymbol{\theta}(i), \mathbf{f}_D(i)]^T$ and $\boldsymbol{\gamma}_j = [\boldsymbol{\phi}(j), \boldsymbol{\theta}(j), \mathbf{f}_D(j)]^T$. The derivations of $\partial \boldsymbol{\mu} / \partial \boldsymbol{\gamma}_i$ and $\partial \boldsymbol{\mu} / \partial \boldsymbol{\gamma}_j$ can be obtained by using the derivation of their general expression $\partial \boldsymbol{\mu} / \partial \boldsymbol{\gamma}_k = [\partial \boldsymbol{\mu} / \partial \boldsymbol{\psi}(k), \partial \boldsymbol{\mu} / \partial \mathbf{f}_D(k)]^T$,

where $\boldsymbol{\psi}(k) \in \{\boldsymbol{\theta}(k), \boldsymbol{\phi}(k)\}$ and the elements in $\partial \boldsymbol{\mu} / \partial \boldsymbol{\gamma}_k$ can be evaluated as

$$\frac{\partial \boldsymbol{\mu}}{\partial \boldsymbol{\psi}(k)} = \left\{ \left[\frac{\partial \mathbb{E}[\mathbf{a}(\boldsymbol{\phi}_k, \boldsymbol{\theta}_k)]}{\partial \boldsymbol{\psi}(k)} \omega_k(t_1) \right]^T, \dots, \left[\frac{\partial \mathbb{E}[\mathbf{a}(\boldsymbol{\phi}_k, \boldsymbol{\theta}_k)]}{\partial \boldsymbol{\psi}(k)} \omega_k(t_L) \right]^T \right\}^T, \quad (27a)$$

$$\frac{\partial \boldsymbol{\mu}}{\partial \mathbf{f}_D(k)} = \left\{ \left[\mathbb{E}[\mathbf{a}(\boldsymbol{\phi}_k, \boldsymbol{\theta}_k)] \frac{\partial \omega_k(t_1)}{\partial \mathbf{f}_D(k)} \right]^T, \dots, \left[\mathbb{E}[\mathbf{a}(\boldsymbol{\phi}_k, \boldsymbol{\theta}_k)] \frac{\partial \omega_k(t_L)}{\partial \mathbf{f}_D(k)} \right]^T \right\}^T. \quad (27b)$$

where $\omega_k(t_l) = e^{j2\pi f_{D,k}t_l/f_s}$. It is noteworthy to highlight that in order to obtain (27), the fact that

$$\frac{\partial \mathbb{E}[\mathbf{a}(\phi_p, \theta_p)]}{\partial \psi(k)} \omega_p(t_l) = 0 \text{ and } \mathbb{E}[\mathbf{a}(\phi_p, \theta_p)] \frac{\partial \omega_p(t_l)}{\partial \mathbf{f}_D(k)} = 0 \forall p \neq k \text{ have been employed.}$$

Define the t_l -th item in $\partial \boldsymbol{\mu} / \partial \psi(k)$ and $\partial \boldsymbol{\mu} / \partial \mathbf{f}_D(k)$ as $\boldsymbol{\ell}_{\psi_k}$ and $\boldsymbol{\ell}_{f_{D,k}}$, respectively, which can be expressed as

$$\boldsymbol{\ell}_{\psi_k} = \boldsymbol{\Lambda}_{\psi_k} \mathbb{E}[\mathbf{a}(\phi_k, \theta_k)] \omega_k(t_l), \quad (28a)$$

$$\boldsymbol{\ell}_{f_{D,k}} = j2\pi t_l / f_s \mathbb{E}[\mathbf{a}(\phi_k, \theta_k)] \omega_k(t_l), \quad (28b)$$

where $\boldsymbol{\Lambda}_{\psi_k}$ indicates the diagonal matrices, which is defined as

$$\boldsymbol{\Lambda}_{\psi_k} \triangleq \text{diag}[\Lambda_{1,1}, \dots, \Lambda_{M,N}], \quad (29)$$

where $\Lambda_{m,n} \in \{\tilde{\Phi}_{m,n}, \tilde{\Gamma}_{m,n}\}$, which can be written as

$$\tilde{\Phi}_{m,n} = -j2\pi \{ -(m-1)d \sin \phi_k + (n-1)d \cos \phi_k \} \sin \theta_k / \lambda, \quad (30a)$$

$$\tilde{\Gamma}_{m,n} = -j2\pi \{ (m-1)d \cos \phi_k + (n-1)d \sin \phi_k \} \cos \theta_k / \lambda. \quad (30b)$$

IV. STAGE II: INFORMATION COMMUNICATION

A. Uplink Communication with MRC

In the communication stage, a novel approach for decoding the transmitted information from the received signal vector in (4). To begin, the estimated location parameters by various localisation algorithms are utilised to infer the channel responses. Afterwards, the MRC technique is adopted to combine the signals using the estimated channel responses to improve the received signal quality, which can be achieved by multiplying $\bar{\mathbf{y}}$ by $\hat{\mathbf{A}} \hat{\mathbf{W}}^H$. Consequently, the obtained communication signal after being processed using MRC, i.e., $\mathbf{x} \in \mathbb{C}^{K \times 1}$, can be expressed as [10]

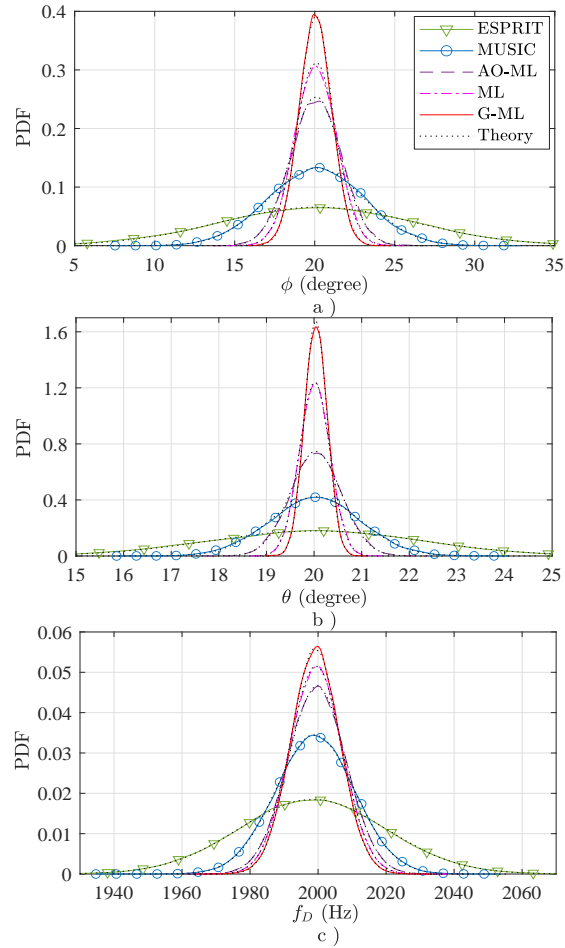


Fig. 2. PDF of the estimated a) Azimuth angle ϕ , b) Elevation angles θ and c) Doppler frequency f_D by various localisation algorithms.

$$\begin{aligned} \mathbf{x} &= (\hat{\mathbf{A}}\hat{\mathbf{W}})^H \bar{\mathbf{y}} \\ &= (\hat{\mathbf{A}}\hat{\mathbf{W}})^H \mathbf{A}\mathbf{W}_s + (\hat{\mathbf{A}}\hat{\mathbf{W}})^H \bar{\mathbf{n}}, \end{aligned} \quad (31)$$

where $\hat{\mathbf{A}}$ and $\hat{\mathbf{W}}$ are respectively given by $\hat{\mathbf{A}} = [\mathbf{a}(\hat{\phi}_1, \hat{\theta}_1), \dots, \mathbf{a}(\hat{\phi}_K, \hat{\theta}_K)]$ and $\hat{\mathbf{W}} \triangleq \text{diag}(e^{j2\pi\hat{f}_{D,1}/f_s}, \dots, e^{j2\pi\hat{f}_{D,K}/f_s})$, respectively. The estimated steering vector associated with the k th drone, i.e., $\mathbf{a}(\hat{\phi}_k, \hat{\theta}_k)$, can be

written as

$$\mathbf{a}(\hat{\phi}_k, \hat{\theta}_k) = \{1, \dots, e^{-j2\pi[(M-1)d \cos\hat{\phi}_k + (N-1)d \sin\hat{\phi}_k] \sin\hat{\theta}_k / \lambda}\}_J, \quad (32)$$

where $\hat{\phi}_k$, $\hat{\theta}_k$ and $\hat{f}_{D,k}$ indicate the azimuth angle, elevation angle and Doppler frequency estimated by the localisation algorithms, which follow Gaussian distributions, as shown in Fig. 2. This figure illustrates the PDF of the estimated azimuth-elevation angles and Doppler frequency of a drone, which is located at $(\phi, \theta, f_D) =$

[(20°, 20°, 2000 Hz), by using $t_L = 100$ pilot signals at the MIMO-BS using $M \times N = 8 \times 8$ antennas with gain-phase defects at SNR = 3 dB. In this figure, the scale parameter of the Rician distributed gain defects is set to $\nu = 0.6$ and the concentration parameter of the von Mises distributed phase defects is set to $\tilde{k} = 10$. In addition, the PDF of the estimated location parameters is compared with the real Gaussian PDF with the same mean and variance as those of the estimated parameters. It can be observed from Fig. 2 that the PDFs of the estimated location parameters and the Gaussian distribution match very well, which indicates these estimated parameters follow the real Gaussian distributions. Moreover, the PDFs of the estimated parameters have nearly identical means, which are very close to the actual values of location parameters, but have different variances. For example, the means of the estimated elevation angles by MUSIC and AO-ML are 20.0210 and 20.0361 degrees, respectively. This is due to the fact that these localisation algorithms are all unbiased estimation algorithms, but their estimation performance varies.

In (31), the k th element of \mathbf{x} can be written as

$$x = \hat{\boldsymbol{\varsigma}}_k^H \boldsymbol{\varsigma}_k s_1 + \sum_{p=1, p \neq k}^K \hat{\boldsymbol{\varsigma}}_k^H \boldsymbol{\varsigma}_p s_p + \hat{\boldsymbol{\varsigma}}_k^H \bar{\mathbf{n}}, \quad (33)$$

where $\hat{\boldsymbol{\varsigma}}_k = \hat{\mathbf{A}}(k) \hat{\mathbf{W}}(k)$, $\boldsymbol{\varsigma}_k = \mathbf{A}(k) \mathbf{W}(k)$ and $\boldsymbol{\varsigma}_p = \mathbf{A}(p) \text{diag}(\boldsymbol{\omega}(p))$. Thus the instantaneous signal-to-interference-plus-noise ratio (SINR) of the k th drone can be represented as

$$\gamma_k = \frac{|\hat{\boldsymbol{\varsigma}}_k^H \boldsymbol{\varsigma}_k|^2}{\sum_{p=1, p \neq k}^K |\hat{\boldsymbol{\varsigma}}_k^H \boldsymbol{\varsigma}_p|^2 + |\hat{\boldsymbol{\varsigma}}_k^H \bar{\mathbf{n}}|^2}, \quad (34)$$

where $\hat{\boldsymbol{\varsigma}}_k^H \boldsymbol{\varsigma}_k = \sum_{m=1}^M \sum_{n=1}^N \hat{h}_{km,n}$, $\hat{\boldsymbol{\varsigma}}_k^H \boldsymbol{\varsigma}_p = \sum_{m=1}^M \sum_{n=1}^N \hat{h}_{pm,n}$ and $\hat{\boldsymbol{\varsigma}}_k^H \bar{\mathbf{n}} = \sum_{m=1}^M \sum_{n=1}^N \hat{h}_{\bar{n}m,n}$, where $\hat{h}_{\bar{n}m,n}$, $\hat{h}_{km,n}$ and $\hat{h}_{pm,n}$ are given

by

$$\hat{h}_{\bar{n}_{m,n}} = \hat{\xi}_{m,n} \bar{n}_{m,n}, \quad (35a)$$

$$\hat{h}_{k,m,n} = \alpha_{m,n} e^{j\Delta\delta_{m,n}} \xi_{m,n} \hat{\xi}_{m,n} e^{j2\pi(f_{D,k} - \hat{f}_{D,k})/f_s}, \quad (35b)$$

$$\hat{h}_{p,m,n} = \alpha_{m,n} e^{j\Delta\delta_{m,n}} \zeta_{m,n} \hat{\xi}_{m,n} e^{j2\pi(f_{D,p} - \hat{f}_{D,k})/f_s}, \quad (35c)$$

where $\bar{n}_{m,n}$ indicates the (m, n) th element of $\bar{\mathbf{n}}$, $\xi_{m,n}$, $\hat{\xi}_{m,n}$ and $\zeta_{m,n}$ are respectively obtained by substituting

$z = m$ and $v = n$ into their general expression $\xi_{z,v}$, $\hat{\xi}_{z,v}$ and $\zeta_{z,v}$, which are

$$\xi_{z,v} = e^{-j2\pi/\lambda\{(z-1)d \cos \phi_k + (v-1)d \sin \phi_k\} \sin \theta_k}, \quad (36a)$$

$$\hat{\xi}_{z,v} = e^{j2\pi/\lambda\{(z-1)d \cos \hat{\phi}_k + (v-1)d \sin \hat{\phi}_k\} \sin \hat{\theta}_k}, \quad (36b)$$

$$\zeta_{z,v} = e^{-j2\pi/\lambda\{(z-1)d \cos \phi_p + (v-1)d \sin \phi_p\} \sin \theta_p}, \quad (36c)$$

Based on (34), the uplink sum rate can be obtained using $R = \sum_{k=1}^K R_k$, where R_k denotes the average data

rate for the k th user, which can be calculated using $R_k = \mathbb{E}\{\log_2(1 + \gamma_k)\}$.

B. An Approximation Method for the Average Data Rate

Due to the fact that the numerator and denominator of γ_k are correlated, directly calculating the closed-form expression for R_k is not feasible as the distribution of γ_k is not traceable. However, using the second-order

Taylor approximation of $\mathbb{E}[\log_2(1 + \gamma_k)]$, we obtain

$$\mathbb{E}[\log_2(1 + \gamma_k)] \approx \log_2(1 + \mathbb{E}[\gamma_k]) - \frac{\mathbb{E}[\gamma_k^2] - \mathbb{E}[\gamma_k]^2}{2 \ln(2)(1 + \mathbb{E}[\gamma_k])^2}, \quad (37)$$

Nevertheless, since $\mathbb{E}[\gamma_k]$ and $\mathbb{E}[\gamma_k^2]$ are still intractable, the second-order Taylor approximation is employed

as well to obtain approximations for them, which are denoted by

$$\mathbb{E}[\gamma_k] \approx \frac{\mathbb{E}[\varsigma_x]}{\mathbb{E}[\varsigma_y]} - \frac{\text{cov}(\varsigma_x, \varsigma_y)}{\mathbb{E}[\varsigma_y]^2} + \frac{\text{var}(\varsigma_y)\mathbb{E}[\varsigma_x]}{\mathbb{E}[\varsigma_y]^3}, \quad (38a)$$

$$\mathbb{E}[\gamma_k^2] \approx \frac{\mathbb{E}[\varsigma_x]^2}{\mathbb{E}[\varsigma_y]^2} + \frac{\text{var}(\varsigma_x)}{\mathbb{E}[\varsigma_y]^2} - \frac{4\mathbb{E}[\varsigma_x]\text{cov}(\varsigma_x, \varsigma_y)}{\mathbb{E}[\varsigma_y]^3} + \frac{3\mathbb{E}[\varsigma_x]^2\text{var}(\varsigma_y)}{\mathbb{E}[\varsigma_y]^4}, \quad (38b)$$

where $\varsigma_x = |\hat{\zeta}_k^H \varsigma_k|^2$ and $\varsigma_y = \sum_{p=1, p \neq k} |\hat{\zeta}_k^H \varsigma_p|^2 + |\hat{\zeta}_k^H \bar{\mathbf{n}}|^2$. The values of $\text{var}(\varsigma_x)$, $\text{var}(\varsigma_y)$ and $\text{cov}(\varsigma_x, \varsigma_y)$ can

be calculated by

$$\text{var}(\varsigma) = \mathbb{E}[\varsigma^2] - \mathbb{E}[\varsigma]^2, \quad (39a)$$

$$\text{cov}(\varsigma_x, \varsigma_y) = \mathbb{E}[\varsigma_x \varsigma_y] - \mathbb{E}[\varsigma_x] \mathbb{E}[\varsigma_y], \quad (39b)$$

where $\varsigma \in \{\varsigma_x, \varsigma_y\}$. Due to the linearity of expectation,

$$\mathbb{E}[\varsigma_y] = \sum_{p=1, p \neq k}^K \mathbb{E}[|\hat{\varsigma}_k^H \varsigma_p|^2] + \mathbb{E}[|\hat{\varsigma}_k^H \bar{\mathbf{n}}|^2], \quad (40)$$

where each item on the right side of (39a), (39b) and (40) will be calculated one by one.

By substituting the values of $\hat{h}_{\tilde{n}, m, n}$, $\hat{h}_{k, m, n}$ and $\hat{h}_{p, m, n}$ from (35a), (35b) and (35c) into $\hat{\varsigma}_k^H \varsigma_k$, $\hat{\varsigma}_k^H \varsigma_p$ and $\hat{\varsigma}_k^H \bar{\mathbf{n}}$,

$\mathbb{E}[\varsigma_x]$ in (39a), $\mathbb{E}[|\hat{\varsigma}_k^H \varsigma_p|^2]$ and $\mathbb{E}[|\hat{\varsigma}_k^H \bar{\mathbf{n}}|^2]$ in (40) can be given by

$$\mathbb{E}[\varsigma_x] = \sum_{m=1}^M \sum_{n=1}^N \sum_{\tilde{m}=1}^M \sum_{\tilde{n}=1}^N \xi_{m,n} \xi_{\tilde{m}, \tilde{n}}^* \mathbb{E}[\alpha_{m,n} \alpha_{\tilde{m}, \tilde{n}}] \mathbb{E}[e^{j(\Delta\delta_{m,n} - \Delta\delta_{\tilde{m}, \tilde{n}})}] \mathbb{E}_{\hat{\xi}_1}, \quad (41a)$$

$$\mathbb{E}[|\hat{\varsigma}_k^H \varsigma_p|^2] = \sum_{m=1}^M \sum_{n=1}^N \sum_{\tilde{m}=1}^M \sum_{\tilde{n}=1}^N \zeta_{m,n} \zeta_{\tilde{m}, \tilde{n}}^* \mathbb{E}[\alpha_{m,n} \alpha_{\tilde{m}, \tilde{n}}] \mathbb{E}[e^{j(\Delta\delta_{m,n} - \Delta\delta_{\tilde{m}, \tilde{n}})}] \mathbb{E}_{\hat{\xi}_1}, \quad (41b)$$

$$\mathbb{E}[|\hat{\varsigma}_k^H \bar{\mathbf{n}}|^2] = \sum_{m=1}^M \sum_{n=1}^N \sum_{\tilde{m}=1}^M \sum_{\tilde{n}=1}^N \mathbb{E}[\bar{n}_{m,n} \bar{n}_{\tilde{m}, \tilde{n}}^*] \mathbb{E}_{\hat{\xi}_1}. \quad (41c)$$

where $\xi_{\tilde{m}, \tilde{n}}$, $\hat{\xi}_{\tilde{m}, \tilde{n}}$, and $\zeta_{\tilde{m}, \tilde{n}}$ can be obtained by substituting $z = \tilde{m}$ and $v = \tilde{n}$ into (36a), (36b) and (36c),

respectively, and $\mathbb{E}_{\hat{\xi}_1} = \mathbb{E}[\hat{\xi}_{m,n} \hat{\xi}_{\tilde{m}, \tilde{n}}^*]$, which can also be written as

$$\mathbb{E}_{\hat{\xi}_1} = \mathbb{E}[e^{j2\pi/\lambda \{ (m-\tilde{m})d \cos \hat{\phi}_k + (n-\tilde{n})d \sin \hat{\phi}_k \} \sin \hat{\theta}_k}], \quad (42)$$

It is worth noting that when $m \neq \tilde{m}$ or $n \neq \tilde{n}$, $\mathbb{E}[|\hat{\varsigma}_k^H \bar{\mathbf{n}}|^2] = 0$ as $\mathbb{E}[\bar{n}_{m,n} \bar{n}_{\tilde{m}, \tilde{n}}^*] = \mathbb{E}[\bar{n}_{m,n}] \mathbb{E}[\bar{n}_{\tilde{m}, \tilde{n}}^*] = 0$

are obtained. In addition, since gain-phase defects are independent across different antennas, $\mathbb{E}[\alpha_{m,n} \alpha_{\tilde{m}, \tilde{n}}] =$

$\mathbb{E}[\alpha_{m,n}] \mathbb{E}[\alpha_{\tilde{m}, \tilde{n}}]$, $\mathbb{E}[e^{j(\Delta\delta_{m,n} - \Delta\delta_{\tilde{m}, \tilde{n}})}] = \mathbb{E}[e^{j\Delta\delta_{m,n}}] \mathbb{E}[e^{-j\Delta\delta_{\tilde{m}, \tilde{n}}}]$. The closed-form expressions of $\mathbb{E}[\alpha_{m,n}]$ and

$\mathbb{E}[\alpha_{\tilde{m}, \tilde{n}}]$ can be obtained by using Theorem 1. Thereafter, the closed-form expressions of $\mathbb{E}[e^{j\Delta\delta_{m,n}}]$ and

$\mathbb{E}[e^{-j\Delta\delta_{\tilde{m}, \tilde{n}}}]$ can be obtained by utilising the derivations of their general expression $\mathbb{E}[e^{\pm jC\Delta\delta_a}]$ in Appendix

A, whilst the derivations of the closed-form expressions of $\mathbb{E}_{\hat{\xi}_1}$ can be found in Appendix B.

Moreover, it can be noticed that $\mathbb{E}[e^{j(\Delta\delta_{m,n}-\Delta\delta_{\tilde{m},\tilde{n}})}] = 1$, $\mathbb{E}_{\hat{\xi}_1} = 1$, $\xi_{m,n}\xi_{\tilde{m},\tilde{n}}^* = 1$ and $\zeta_{m,n}\zeta_{\tilde{m},\tilde{n}}^* = 1$ in (41)

when $m = \tilde{m}$ and $n = \tilde{n}$. Consequently,

$$\mathbb{E}[|\hat{\varsigma}_k^H \bar{\mathbf{n}}|^2] = \sum_{m=1}^M \sum_{n=1}^N \sum_{\tilde{m}=1}^M \sum_{\tilde{n}=1}^N \mathbb{E}[\bar{n}_{m,n}^2], \quad (43a)$$

$$\mathbb{E}[\varsigma_x] = \mathbb{E}[|\hat{\varsigma}_k^H \varsigma_p|^2] = \sum_{m=1}^M \sum_{n=1}^N \sum_{\tilde{m}=1}^M \sum_{\tilde{n}=1}^N \mathbb{E}[\alpha_{m,n}^2], \quad (43b)$$

where the derivations of the closed-form expression of $\mathbb{E}[\alpha_{m,n}^2]$ can be found in Theorem 1.

Using the the linearity of expectation, $\mathbb{E}[\varsigma_x \varsigma_y]$ in (39b) can also be obtained, which is expressed as

$$\mathbb{E}[\varsigma_x \varsigma_y] = \sum_{p=1, p \neq k}^K \mathbb{E}[|\hat{\varsigma}_k^H \varsigma_k|^2 |\hat{\varsigma}_k^H \varsigma_p|^2] + \mathbb{E}[|\hat{\varsigma}_k^H \varsigma_k|^2 |\hat{\varsigma}_k^H \bar{\mathbf{n}}|^2], \quad (44)$$

The terms $\mathbb{E}[|\hat{\varsigma}_k^H \varsigma_k|^2 |\hat{\varsigma}_k^H \varsigma_p|^2]$ and $\mathbb{E}[|\hat{\varsigma}_k^H \varsigma_k|^2 |\hat{\varsigma}_k^H \bar{\mathbf{n}}|^2]$ in (44) can be respectively evaluated as

$$\mathbb{E}[|\hat{\varsigma}_k^H \varsigma_k|^2 |\hat{\varsigma}_k^H \varsigma_p|^2] = \sum_{m_1=1}^M \sum_{n_1=1}^N \sum_{\tilde{m}_1=1}^M \sum_{\tilde{n}_1=1}^N \sum_{m_2=1}^M \sum_{n_2=1}^N \sum_{\tilde{m}_2=1}^M \sum_{\tilde{n}_2=1}^N \mathbb{E}_1, \quad (45a)$$

$$\mathbb{E}[|\hat{\varsigma}_k^H \varsigma_k|^2 |\hat{\varsigma}_k^H \bar{\mathbf{n}}|^2] = \sum_{m_1=1}^M \sum_{n_1=1}^N \sum_{\tilde{m}_1=1}^M \sum_{\tilde{n}_1=1}^N \sum_{m_2=1}^M \sum_{n_2=1}^N \sum_{\tilde{m}_2=1}^M \sum_{\tilde{n}_2=1}^N \mathbb{E}_2, \quad (45b)$$

where \mathbb{E}_1 and \mathbb{E}_2 can be written as

$$\mathbb{E}_1 = \xi_{m_1, n_1} \xi_{\tilde{m}_1, \tilde{n}_1}^* \zeta_{m_2, n_2} \zeta_{\tilde{m}_2, \tilde{n}_2}^* \mathbb{E}_\alpha \mathbb{E}_\delta \mathbb{E}_{\hat{\xi}_2}, \quad (46a)$$

$$\mathbb{E}_2 = \xi_{m_1, n_1} \xi_{\tilde{m}_1, \tilde{n}_1}^* \mathbb{E}[\alpha_{m_1, n_1} \alpha_{\tilde{m}_1, \tilde{n}_1}] \mathbb{E}[\bar{n}_{m_2, n_2} \bar{n}_{\tilde{m}_2, \tilde{n}_2}^*] \mathbb{E}[e^{j(\Delta\delta_{m_1, n_1} - \Delta\delta_{\tilde{m}_1, \tilde{n}_1})}] \mathbb{E}_{\hat{\xi}_2}, \quad (46b)$$

where ξ_{m_1, n_1} and $\xi_{\tilde{m}_1, \tilde{n}_1}$ can be obtained by substituting $z = m_1, v = n_1$ and $z = \tilde{m}_1, v = \tilde{n}_1$ into (36a),

respectively, whilst ζ_{m_2, n_2} and $\zeta_{\tilde{m}_2, \tilde{n}_2}^*$ can be obtained by substituting $z = m_2, v = n_2$ and $z = \tilde{m}_2, v = \tilde{n}_2$

into (36c), respectively. The terms \mathbb{E}_α and \mathbb{E}_δ are respectively given by

$$\mathbb{E}_\alpha = \mathbb{E}[\alpha_{m_1, n_1} \alpha_{m_2, n_2} \alpha_{\tilde{m}_1, \tilde{n}_1} \alpha_{\tilde{m}_2, \tilde{n}_2}], \quad (47a)$$

$$\mathbb{E}_\delta = \mathbb{E}[e^{j(\Delta\delta_{m_1, n_1} + \Delta\delta_{m_2, n_2} - \Delta\delta_{\tilde{m}_1, \tilde{n}_1} - \Delta\delta_{\tilde{m}_2, \tilde{n}_2})}]. \quad (47b)$$

In addition, $\mathbb{E}_{\hat{\xi}_2} = \mathbb{E}[\hat{\xi}_{m_1, n_1} \hat{\xi}_{\tilde{m}_1, \tilde{n}_1}^* \hat{\xi}_{m_2, n_2} \hat{\xi}_{\tilde{m}_2, \tilde{n}_2}^*]$, which is

$$\mathbb{E}_{\hat{\xi}_2} = \mathbb{E}[e^{j2\pi/\lambda\{(m_1+m_2-\tilde{m}_1-\tilde{m}_2)d \cos \hat{\phi}_k + (n_1+n_2-\tilde{n}_1-\tilde{n}_2)d \sin \hat{\phi}_k\} \sin \hat{\theta}_k}], \quad (48)$$

where $\hat{\xi}_{m_1, n_1}$, $\hat{\xi}_{m_2, n_2}$, $\hat{\xi}_{\tilde{m}_1, \tilde{n}_1}^*$ and $\hat{\xi}_{\tilde{m}_2, \tilde{n}_2}^*$ can be obtained respectively by substituting different values of z and

v into (36b).

In (46), the derivations of $\mathbb{E}[\alpha_{m_1, n_1} \alpha_{\tilde{m}_1, \tilde{n}_1}]$ and \mathbb{E}_α are similar to that of $\mathbb{E}[\alpha_{m, n} \alpha_{\tilde{m}, \tilde{n}}]$, whilst the derivations of $\mathbb{E}[e^{j(\Delta\delta_{m_1, n_1} - \Delta\delta_{\tilde{m}_1, \tilde{n}_1})}]$ and \mathbb{E}_δ are similar to that of $\mathbb{E}[e^{j(\Delta\delta_{m, n} - \Delta\delta_{\tilde{m}, \tilde{n}})}]$. In addition, the derivations of $\mathbb{E}[\bar{n}_{m_2, n_2} \bar{n}_{\tilde{m}_2, \tilde{n}_2}^*]$ and $\mathbb{E}_{\hat{\xi}_2}$ are similar to that of $\mathbb{E}[\bar{n}_{m, n} \bar{n}_{\tilde{m}, \tilde{n}}^*]$ and $\mathbb{E}_{\hat{\xi}_1}$, respectively. The calculations of the expectations above all depend on whether the individual terms inside the expectation are the same or not. The complete derivations of the closed-form expression of $\mathbb{E}_{\hat{\xi}_2}$ can be found in Appendix B.

Then $\mathbb{E}[\varsigma_x^2]$ in (39a) can be given by $\mathbb{E}[\varsigma_x^2] = \sum_{m_1=1}^M \sum_{n_1=1}^N \sum_{\tilde{m}_1=1}^M \sum_{\tilde{n}_1=1}^N \sum_{m_2=1}^M \sum_{n_2=1}^N \sum_{\tilde{m}_2=1}^M \sum_{\tilde{n}_2=1}^N \mathbb{E}_3$, where

$$\mathbb{E}_3 = \xi_{m_1, n_1} \xi_{\tilde{m}_1, \tilde{n}_1}^* \xi_{m_2, n_2} \xi_{\tilde{m}_2, \tilde{n}_2}^* \mathbb{E}_\alpha \mathbb{E}_\delta \mathbb{E}_{\hat{\xi}_2}. \quad (49)$$

On the other hand, $\mathbb{E}[\varsigma_y^2]$ in (39a) can be expressed as

$$\mathbb{E}[\varsigma_y^2] = \mathbb{E}[\varsigma_{y1}^2] + 2\mathbb{E}[\varsigma_{y1} \varsigma_{y2}] + \mathbb{E}[\varsigma_{y2}^2], \quad (50)$$

where $\varsigma_{y1} = \sum_{p=1, p \neq k}^K |\hat{\varsigma}_k^H \varsigma_p|^2$ and $\varsigma_{y2} = |\hat{\varsigma}_k^H \bar{\mathbf{n}}|^2$. By performing some algebraic manipulations, $\mathbb{E}[\varsigma_{y2}^2]$,

$\mathbb{E}[\varsigma_{y1} \varsigma_{y2}]$ and $\mathbb{E}[\varsigma_{y1}^2]$ can be respectively given by

$$\mathbb{E}[\varsigma_{y2}^2] = \mathbb{E}[(|\hat{\varsigma}_k^H \bar{\mathbf{n}}|^2)^2], \quad (51a)$$

$$\mathbb{E}[\varsigma_{y1} \varsigma_{y2}] = \sum_{p=1, p \neq k}^K \mathbb{E}[|\hat{\varsigma}_k^H \varsigma_p|^2 |\hat{\varsigma}_k^H \bar{\mathbf{n}}|^2], \quad (51b)$$

$$\mathbb{E}[\varsigma_{y1}^2] = \sum_{p=1, p \neq k}^K \mathbb{E}[(|\hat{\varsigma}_k^H \varsigma_p|^2)^2] + 2 \sum_{p < \tilde{p}, p \neq k, \tilde{p} \neq k}^K \mathbb{E}[|\hat{\varsigma}_k^H \varsigma_p|^2 |\hat{\varsigma}_k^H \varsigma_{\tilde{p}}|^2], \quad (51c)$$

where $\mathbb{E}[(|\hat{\varsigma}_k^H \varsigma_p|^2)^2]$, $\mathbb{E}[|\hat{\varsigma}_k^H \varsigma_p|^2 |\hat{\varsigma}_k^H \varsigma_{\tilde{p}}|^2]$, $\mathbb{E}[|\hat{\varsigma}_k^H \varsigma_p|^2 |\hat{\varsigma}_k^H \bar{\mathbf{n}}|^2]$ and $\mathbb{E}[(|\hat{\varsigma}_k^H \bar{\mathbf{n}}|^2)^2]$ can be denoted by using the

general expression $\mathbb{E}[\varsigma_{\bar{\vartheta}}]$ for $\bar{\vartheta} \in \{a, b, c, d\}$, which is given by $\mathbb{E}[\varsigma_{\bar{\vartheta}}] = \sum_{m_1=1}^M \sum_{n_1=1}^N \sum_{\tilde{m}_1=1}^M \sum_{\tilde{n}_1=1}^N \sum_{m_2=1}^M \sum_{n_2=1}^N \sum_{\tilde{m}_2=1}^M \sum_{\tilde{n}_2=1}^N \mathbb{E}_{\bar{\vartheta}}$,

where $\varsigma_a = (|\hat{\varsigma}_k^H \varsigma_p|^2)^2$, $\varsigma_b = |\hat{\varsigma}_k^H \varsigma_p|^2 |\hat{\varsigma}_k^H \varsigma_{\bar{p}}|^2$, $\varsigma_c = |\hat{\varsigma}_k^H \varsigma_p|^2 |\hat{\varsigma}_k^H \bar{\mathbf{n}}|^2$ and $\varsigma_d = (|\hat{\varsigma}_k^H \bar{\mathbf{n}}|^2)^2$. In addition, by substituting $\bar{\vartheta}$ with a, b, c , and d , $\mathbb{E}_a, \mathbb{E}_b, \mathbb{E}_c, \mathbb{E}_d$ can be written as

$$\mathbb{E}_a = \zeta_{m_1, n_1} \zeta_{\tilde{m}_1, \tilde{n}_1}^* \zeta_{m_2, n_2} \zeta_{\tilde{m}_2, \tilde{n}_2}^* \mathbb{E}_\alpha \mathbb{E}_\delta \mathbb{E}_{\hat{\xi}_2}, \quad (52a)$$

$$\mathbb{E}_b = \zeta_{m_1, n_1} \zeta_{\tilde{m}_1, \tilde{n}_1}^* \rho_{m_2, n_2} \rho_{\tilde{m}_2, \tilde{n}_2}^* \mathbb{E}_\alpha \mathbb{E}_\delta \mathbb{E}_{\hat{\xi}_2}, \quad (52b)$$

$$\mathbb{E}_c = \zeta_{m_1, n_1} \zeta_{\tilde{m}_1, \tilde{n}_1}^* \mathbb{E}[\alpha_{m_1, n_1} \alpha_{\tilde{m}_1, \tilde{n}_1}] \mathbb{E}[\bar{n}_{m_2, n_2} \bar{n}_{\tilde{m}_2, \tilde{n}_2}^*] \mathbb{E}[e^{j(\Delta\delta_{m_1, n_1} - \Delta\delta_{\tilde{m}_1, \tilde{n}_1})}] \mathbb{E}_{\hat{\xi}_2}, \quad (52c)$$

$$\mathbb{E}_d = \mathbb{E}[\bar{n}_{m_1, n_1} \bar{n}_{\tilde{m}_1, \tilde{n}_1}^* \bar{n}_{m_2, n_2} \bar{n}_{\tilde{m}_2, \tilde{n}_2}^*] \mathbb{E}_{\hat{\xi}_2}, \quad (52d)$$

where ρ_{m_2, n_2} and $\rho_{\tilde{m}_2, \tilde{n}_2}$ can be respectively obtained by substituting $z = m_2, v = n_2$ and $z = \tilde{m}_2, v = \tilde{n}_2$ into $\rho_{z, v}$, which is written as $\rho_{z, v} = e^{-j2\pi/\lambda\{(z-1)d \cos \phi_{\bar{p}} + (v-1)d \sin \phi_{\bar{p}}\} \sin \theta_{\bar{p}}}$. The derivation of $\mathbb{E}[\bar{n}_{m_1, n_1} \bar{n}_{\tilde{m}_1, \tilde{n}_1}^* \bar{n}_{m_2, n_2} \bar{n}_{\tilde{m}_2, \tilde{n}_2}^*]$ is similar to the derivation of $\mathbb{E}[\bar{n}_{m, n} \bar{n}_{\tilde{m}, \tilde{n}}^*]$.

By substituting the calculated results of $\mathbb{E}[\varsigma_y]$ by (40), $\mathbb{E}[\varsigma_x]$ by (41a), $\mathbb{E}[\varsigma_x \varsigma_y]$ by (44), $\mathbb{E}[\varsigma_x^2]$ and $\mathbb{E}[\varsigma_y^2]$ by (50) into (38) to calculate $\mathbb{E}[\gamma_k]$ and $\mathbb{E}[\gamma_k^2]$ and then substituting the obtained results into (37), the approximation value of $\mathbb{E}[\log_2(1 + \gamma_k)]$ can be calculated. It is worth noting that there is no $\hat{f}_{D, k}$ in $\mathbb{E}[\varsigma_x], \mathbb{E}[\varsigma_y], \mathbb{E}[\varsigma_x \varsigma_y], \mathbb{E}[\varsigma_x^2]$ and $\mathbb{E}[\varsigma_y^2]$ as $\hat{f}_{D, k}$ is cancelled out in $|\hat{\varsigma}_k^H \varsigma_k|^2$ and $|\hat{\varsigma}_k^H \varsigma_p|^2$. As a consequence, we can conclude that the average sum data rate $\mathbb{E}[\log_2(1 + \gamma_k)]$ is not affected by the estimation errors of Doppler frequency.

Theorem 1: The c -th central moment of the Rician distribution is given by

$$\mathbb{E}[\alpha_a^c] = \frac{e^{-\frac{\nu^2}{2\sigma_r^2}}}{2\sigma_r^2} \sum_{b=0}^{\infty} \left\{ \frac{\nu^{2b} \left(\frac{1}{2\sigma_r^2}\right)^{b-\frac{c+2}{2}}}{b! \Gamma(b+1)} \gamma\left(\frac{2b+c+2}{2}, \frac{\alpha_{a, \max}^2}{2\sigma_r^2}\right) \right\}, \quad (53)$$

where $\gamma(\cdot)$ denotes a lower incomplete gamma function and $a \in \{\{m, n\}, \{m_1, n_1\}, \{m_2, n_2\}, \{\tilde{m}, \tilde{n}\}, \{\tilde{m}_1, \tilde{n}_1\}, \{\tilde{m}_2, \tilde{n}_2\}, u, v\}$.

Proof: See Appendix A.

V. NUMERICAL RESULTS

In this section, the simulation and analytical results are provided to evaluate the effect of different gain-phase defects on the localisation performance of various algorithms including the ESPRIT and MUSIC algorithms in [20], AO-ML algorithm, ML algorithm, and G-ML, as well as the communication performance using SDR of SPD-MPL and MPD-MPL introduced in Sec. II. In the simulation, a number of $K = 3$ drones with equal distance to a MIMO-BS and located at $(\phi, \theta, f_D) = [(20^\circ, 20^\circ, 2000 \text{ Hz}), (40^\circ, 40^\circ, 4000 \text{ Hz}), (60^\circ, 60^\circ, 6000 \text{ Hz})]$ are considered. The MIMO-BS is equipped with a URA that is composed of $M \times N = 8 \times 8$ antennas. The scale parameter of the Rician distributed gain defects on the MIMO-BS is set to $\sigma_r = 0.1$ for all figures except for Fig. 3 as it does not consider the gain defects. In this case, the effects of gain defects and phase defects on the ISAC system can be controlled by varying the values of ν and \tilde{k} , respectively. The signal wavelength and sampling frequency are $\lambda = 6 \text{ cm}$ and $f_s = 100 \text{ kHz}$, respectively. In addition, the length of the frame in Fig. 1 is $t_L = 100$ subframes, which is equal to the number of pilots per frame. In each simulation, $N_m = 1000$ Monte Carlo tests are performed. The root mean squared error (RMSE) in [40] is employed to evaluate the localisation accuracy of the estimators in stage I, while the SDR is utilised to evaluate the communication performance in stage II.

Fig. 3 demonstrates the performance of the ISAC system considered in this paper without gain-phase defects. Specifically, Fig. 3a, Fig. 3b and Fig. 3c show the estimation performance of the various algorithms for ϕ , θ and f_D , whilst Fig. 3d and Fig. 3e illustrate the achievable SDRs for SPD-MPL and MPD-MPL, which

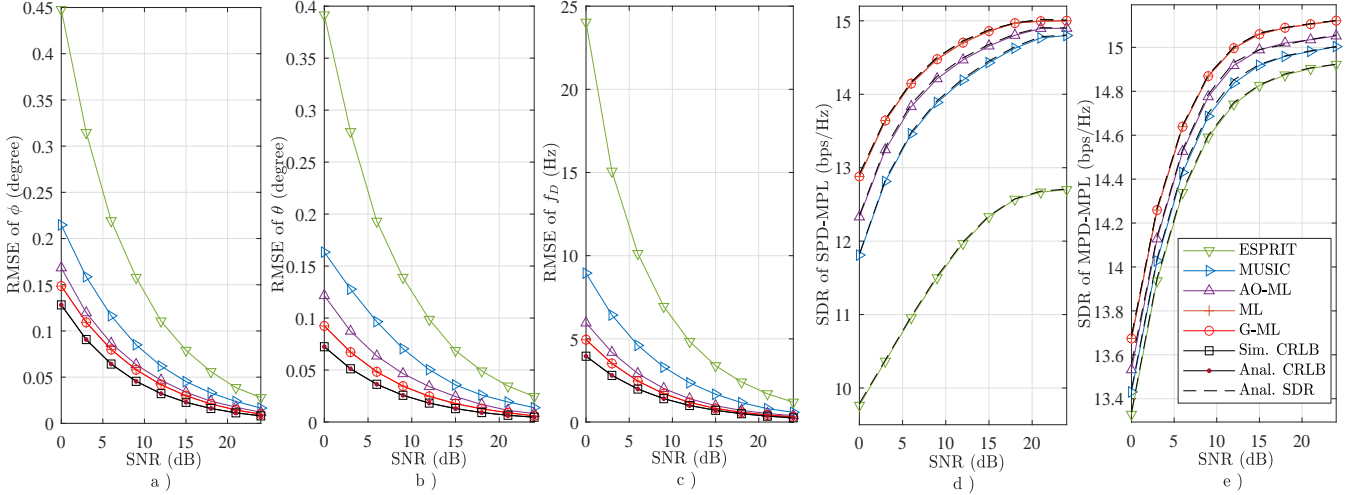


Fig. 3. RMSEs of the a) Azimuth angle ϕ , b) Elevation angle θ , c) Doppler frequency f_D estimations, d) SDR of SPD-MPL, and e) SDR of MPD-MPL without gain-phase errors.

are obtained using MRC with weights calculated based on the parameters estimated by different localisation algorithms. As can be seen from this figure, G-ML and ML exhibit the best performance in terms of both RMSE and SDRs, followed by AO-ML and MUSIC, whilst ESPRIT has the worst performance. The figure also shows that G-ML and ML have the same performance when there are no gain-phase errors. This can be attributed to the fact that the difference between the two algorithms is mainly the assumption about the knowledge of gain-phase errors, and thus they are the same when the system does not suffer from such errors. In addition, the performance gap between AO-ML and the optimal ML is small and this gap is due to the suboptimal AO technique used to optimize the ML function in the AO-ML case. For instance, the difference in the RMSE of the azimuth angle estimated by AO-ML and ML is only 0.0067 degrees when $\text{SNR} = 6$ dB. Fig. 3 shows that when $\text{SNR} \geq 20$ dB, the RMSE of ML, G-ML and AO-ML approaches CRLB, whilst MUSIC and ESPRIT do not approach CRLB in the entire range of the considered SNR. Moreover, since

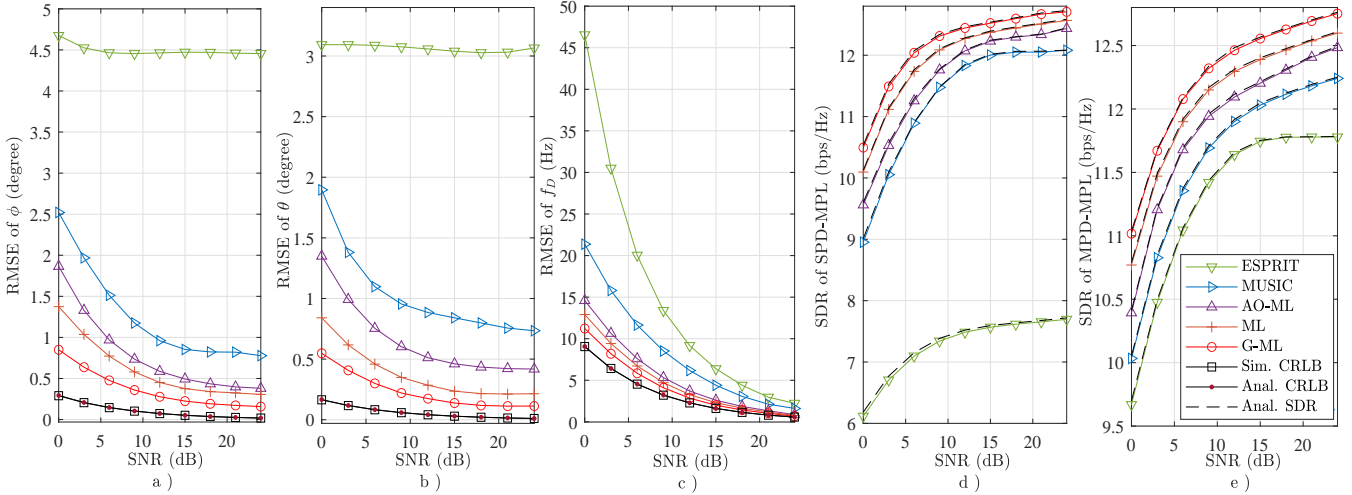


Fig. 4. RMSEs of the a) Azimuth angle ϕ , b) Elevation angle θ , c) Doppler frequency f_D estimations, d) SDR of SPD-MPL, and e) SDR of MPD-MPL with $\nu = 1$ and $\tilde{k} = 2$.

the localisation algorithms in MPD-MPL utilise more pilot signals compared to SPD-MPL, SDRs of MPD-MPL corresponding to all localisation algorithms are larger than SDRs of SPD-MPL, especially for ESPRIT. The figure also shows a perfect match between simulated and derived CRLB and SDRs, which confirms the derivations in this paper.

Fig. 4 demonstrates the effect of gain-phase defects on the localisation and communication performance of the considered ISAC system. In this figure, ν and \tilde{k} are set to $\nu = 1$ and $\tilde{k} = 2$, respectively. By comparing Fig. 4 to Fig. 3, it can be observed that both the localisation and communication performance of the ISAC system is affected by gain-phase defects, especially for the case of ESPRIT, where the azimuth-elevation estimation by the ESPRIT algorithm fails completely. However, the AO-ML algorithm, ML algorithm and G-ML manage to reduce the impact of the gain-phase defects compared to the ESPRIT and MUSIC algorithms. For instance, the RMSE of the elevation angle estimation by AO-ML, ML and G-ML are 0.5116, 0.2844, 0.1742 degrees, which are much lower than that of the elevation angle estimated by ESPRIT and MUSIC, which are 3.0582,

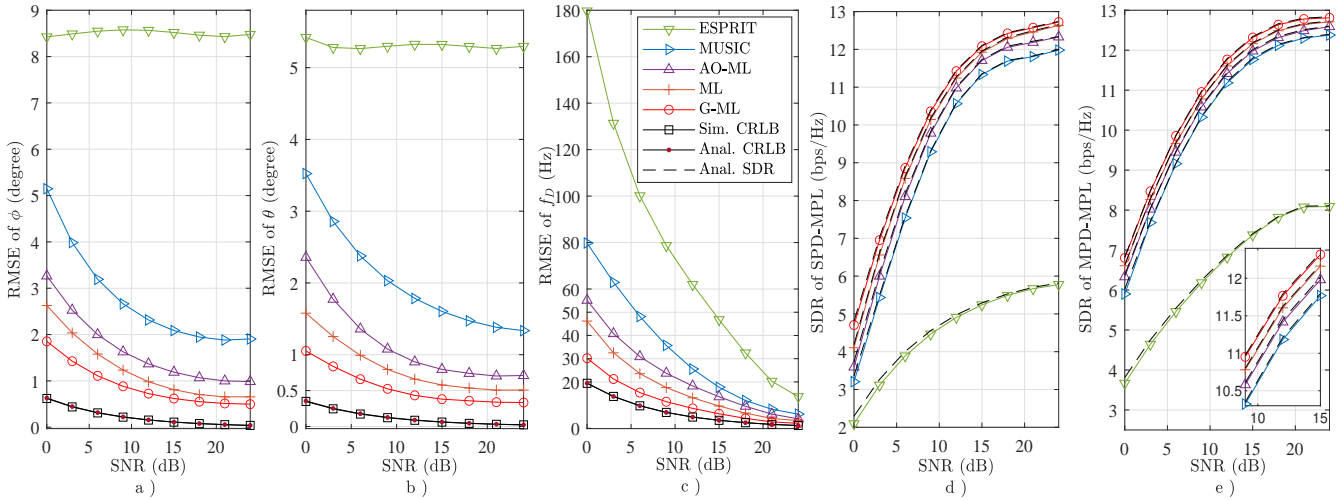


Fig. 5. RMSEs of the a) Azimuth angle ϕ , b) Elevation angle θ , c) Doppler frequency f_D estimations, d) SDR of SPD-MPL, and e) SDR of MPD-MPL with $\nu = 0.3$ and $\tilde{k} = 2$.

0.8845 degrees when $\text{SNR} = 12$ dB. Moreover, the analytical and simulation results of both CRLB and SDRs match very well, which indicates the validity of the analytical results, in addition to the accuracy of the proposed approximation method.

Fig. 5 shows the impact of larger gain defects compared to those of Fig. 4 on the ISAC system, where the value of ν is decreased from 1, as in Fig. 4, to 0.3. In this figure, the value of \tilde{k} is still $\tilde{k} = 2$ so that the impact of phase defects on Fig. 5 is the same as that on Fig. 4. By comparing the results of Fig. 4 and Fig. 5, it can be found that both the communication and localisation performance of the considered ISAC system have become less efficient in Fig. 4 as a response to decreasing ν . For instance, the RMSE of the azimuth angle estimation by MUSIC increases by 1.6804 degrees when ν decreases from 1 to 0.3 at $\text{SNR} = 6$ dB. In addition, the SDR of SPD-MPL obtained after preprocessing the received signals using the estimated location parameters by G-ML reduces by 1.9546 bps/Hz when ν decreases from 1 to 0.3 at $\text{SNR} = 9$ dB. This phenomenon can be attributed to the fact that the further ν deviates from 1, the greater its impact on the system as the ideal value

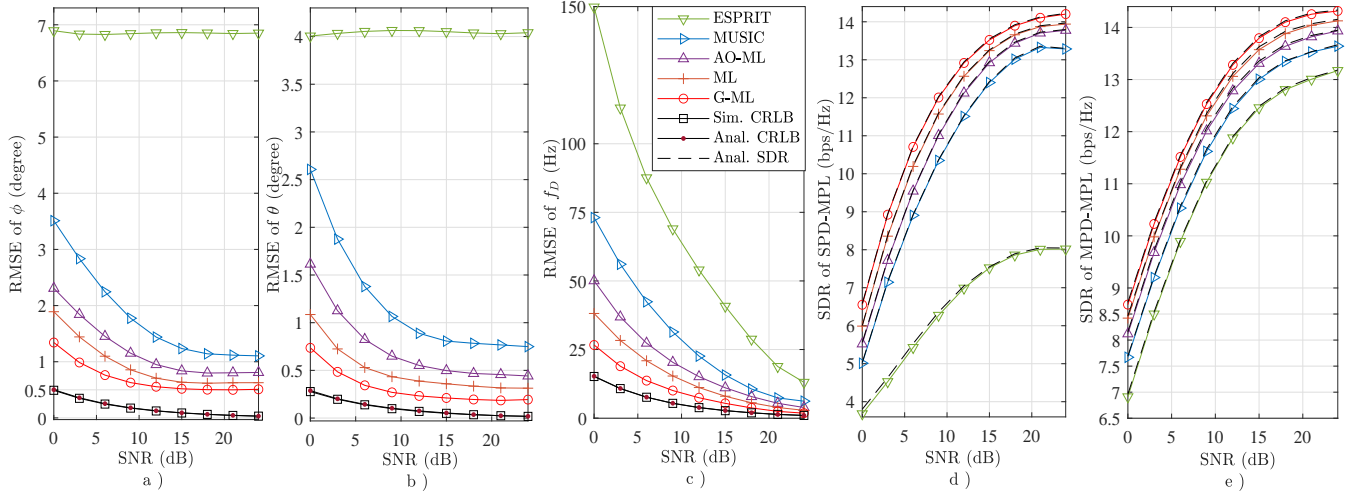


Fig. 6. RMSEs of the a) Azimuth angle ϕ , b) Elevation angle θ , c) Doppler frequency f_D estimations, d) SDR of SPD-MPL, and e) SDR of MPD-MPL with $\nu = 0.3$ and $\tilde{k} = 4$.

of ν for gain imperfections is 1. With the same level of gain defects, the SDRs obtained by using the estimated location parameters from different localisation algorithms may be significantly different. For example, the gap between the SDRs of MPD-MPL obtained by using the estimated location parameters by ESPRIT and G-ML is 4.9278 bps/Hz when $\text{SNR} = 12$ dB. It can also be noted from Fig. 5 that the difference between SDRs of SPD-MPL and MPD-MPL decreases with the increase of SNR, which indicates that high SNR has a negative impact on the performance improvement resulting from the increase of pilot signals. This is because the gap of estimation errors by using different numbers of pilot signals is very small at high SNR.

Fig. 6 demonstrates the effects of changing phase errors on the performance of the considered ISAC system by increasing the value of \tilde{k} from 2 to 4 and adopting the same value of ν as in Fig. 5. By comparing the results of Fig. 6 and Fig. 5, it can be noted that both the communication and localisation performance of the ISAC system in Fig. 6 is improved compared to that in Fig. 5. For instance, the SDR of SPD-MPL obtained by using the estimated location parameters from ML has increased by 1.3249 bps/Hz when $\text{SNR} = 12$ dB and

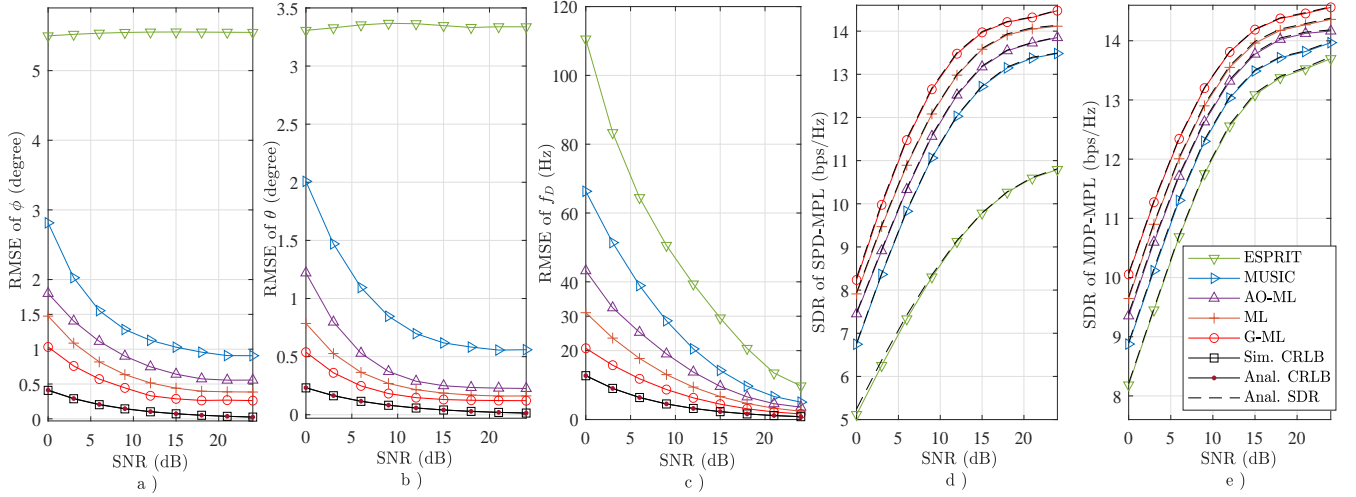


Fig. 7. RMSEs of the a) Azimuth angle ϕ , b) Elevation angle θ , c) Doppler frequency f_D estimations, d) SDR of SPD-MPL, and e) SDR of MPD-MPL with $\nu = 0.3$ and $\tilde{k} = 100$.

the RMSE of the Doppler frequency by ML has decreased from 13.1803 Hz to 11.1403 Hz at the same SNR.

This is due to the fact that the shape of the PDF of the von Mises distribution becomes sharper as \tilde{k} becomes larger, which in turn results in more variables in the von Mises distribution clustering around 0, which is also the ideal case of the phase defects. Furthermore, the analytical and simulation results of both CRLB and SDRs match very well.

Fig. 7 shows the effect of smaller phase defects on the performance of the considered ISAC system by increasing the value of \tilde{k} from 4, as in Fig. 6, to 100, while fixing the value of ν at 0.3. To begin, the analytical results and simulation results of both CRLB and SDRs match very well. Moreover, by comparing the results of Fig. 5, Fig. 6 and Fig. 7, it can be concluded that both the communication and localisation performance of the ISAC system become better with the increase in \tilde{k} . For instance, the RMSE of the elevation angle estimation by AO-ML increases by 0.3279 degrees when $\text{SNR} = 3$ dB. Moreover, by comparing Fig. 5, Fig.

6 and Fig. 7 it can be noted that increasing \tilde{k} from 4 to 100 has a relatively slow performance improvement on the considered ISAC system, especially when compared to the case where \tilde{k} is increased from 2 to 4. For example, the SDR of MPD-MPL obtained by using the estimated location parameters from G-ML has increased by 1.0424 bps/Hz when \tilde{k} increases from 4 to 100 at $\text{SNR} = 3$ dB and increased by 1.7609 bps/Hz when \tilde{k} increases from 2 to 4 at the same SNR.

VI. CONCLUSION

In this paper, an ISAC system consisting of MIMO-BS that performs localisation and data-detection was investigated in two phases under gain-phase defects for two possible scenarios. In the localisation phase, joint estimation for azimuth angle, elevation angle and Doppler frequency of all drones was performed, where RMSE is used as the performance evaluation metric. Several localisation algorithms were adopted including ESPRIT and MUSIC algorithms, in addition to the proposed ML and AO-ML algorithms for the localisation process. Moreover, CRLB with a closed-form expression was derived as a function of the statistics of the gain-phase imperfections. In the second phase, an MRC technique is employed for preprocessing the received communication signal by using the estimated location parameters in the first phase. An accurate closed-form approximation for the achievable average sum data rate was derived. The obtained results revealed that gain-phase errors can have a severe impact on the localisation and communication systems. In addition, it was found that the proposed ML and AO-ML algorithms outperform MUSIC and ESPRIT under many operating conditions and that the RMSE of the ML and AO-ML approaches the CRLB at high SNRs. The validity of

the analytical results was demonstrated by simulations.

APPENDIX A

A PROOF FOR THEOREM 1 AND THE COMPLETE DERIVATION OF $\mathbb{E}[e^{\pm jC\Delta\delta_a}]$

To prove the c -th central moment of the Rician distribution shown in Theorem 1 on page 25, the definition of the expectation is invoked, thus $\mathbb{E}[\alpha_a^c] \forall \alpha_a^c \in [0, \alpha_{a,\max}]$ can be given by

$$\mathbb{E}[\alpha_a^c] = \int_0^{\alpha_{a,\max}} \alpha_a^c f(\alpha_a) d(\alpha_a), \quad (54)$$

where $f(\alpha_a)$ is given in (5). By using the infinite series representation of the modified Bessel function in (6)

and performing some algebraic operations, $\mathbb{E}[\alpha_a^c]$ can be written as

$$\mathbb{E}[\alpha_a^c] = \frac{e^{-\frac{\nu^2}{2\sigma_r^2}}}{\sigma_r^2} \sum_{b=0}^{\infty} \left\{ \frac{1}{b! \Gamma(b+1)} \left(\frac{\nu}{2\sigma_r^2} \right)^{2b} \mathcal{I}_1 \right\}, \quad (55)$$

where

$$\mathcal{I}_1 = \int_0^{\alpha_{a,\max}} \alpha_a^{2b+c+1} e^{-\frac{\alpha_a^2}{2\sigma_r^2}} d(\alpha_a). \quad (56)$$

Afterwards, \mathcal{I}_1 can be solved by using [41, Eq.8, pp. 346] as

$$\mathcal{I}_1 = \frac{1}{2} \left(\frac{1}{2\sigma_r^2} \right)^{-\frac{2b+c+2}{2}} \gamma \left(\frac{2b+c+2}{2}, \frac{\alpha_{a,\max}^2}{2\sigma_r^2} \right), \quad (57)$$

where $\gamma(\tilde{s}, \tilde{x})$ denotes the lower incomplete Gamma function. Afterwards, by substituting the results of (57)

in (55), the closed form of $\mathbb{E}[\alpha_a^c]$ can be obtained, which is given in Theorem 1.

On the other hand, $\mathbb{E}[e^{\pm jC\Delta\delta_a}]$, where $a \in \{\{m, n\}, \{m_1, n_1\}, \{m_2, n_2\}, \{\tilde{m}, \tilde{n}\}, \{\tilde{m}_1, \tilde{n}_1\}, \{\tilde{m}_2, \tilde{n}_2\}, u, v\}$,

can be expressed as

$$\mathbb{E}[e^{\pm jC\Delta\delta_a}] = \int_{\Delta\delta_{a,\min}}^{\Delta\delta_{a,\max}} e^{\pm jC\Delta\delta_a} f(\Delta\delta_a) d\Delta\delta_a, \quad (58)$$

where $f(\Delta\delta_a)$ can be obtained using (8) by substituting $\Delta\delta_{m,n}$ with $\Delta\delta_a$. Substituting (8) in (58), $\mathbb{E}[e^{\pm jC\Delta\delta_a}]$

gives

$$\mathbb{E}[e^{\pm jC\Delta\delta_a}] = \mathcal{I}_2 + \frac{1}{\pi I_0(\tilde{k})} \sum_{q=1}^{\infty} I_q(\tilde{k}) \mathcal{I}_3, \quad (59)$$

where

$$\begin{aligned} \mathcal{I}_2 &= \int_{\Delta\delta_{a,\min}}^{\Delta\delta_{a,\max}} \frac{e^{\pm jC\Delta\delta_a}}{2\pi} d\Delta\delta_a \\ &= \frac{1}{2C\pi} (\pm j e^{\pm jC\Delta\delta_{a,\min}} \mp j e^{\pm jC\Delta\delta_{a,\max}}), \end{aligned} \quad (60)$$

and

$$\mathcal{I}_3 = \int_{\Delta\delta_{a,\min}}^{\Delta\delta_{a,\max}} e^{\pm jC\Delta\delta_a} \cos[q(\Delta\delta_a - \tilde{\mu})] d\Delta\delta_a. \quad (61)$$

To evaluate \mathcal{I}_3 , integration by part of the integral in (61) is performed twice. Thus, the closed-form solution is

given as

$$\mathcal{I}_3 = \mp \frac{1}{q^2 - C^2} (\tau_1 + \tau_2), \quad (62)$$

where

$$\tau_1 = \sum_{\tilde{\ell}=1}^2 (-1)^{\tilde{\ell}+1} j C e^{\pm jC\Delta\delta_{\tilde{\ell}}} \cos(\Delta\delta_{\tilde{\ell}} q - q\tilde{\mu}), \quad (63)$$

and

$$\tau_2 = \sum_{\tilde{\ell}=1}^2 (-1)^{\tilde{\ell}+1} q e^{\pm jC\Delta\delta_{\tilde{\ell}}} \sin(\Delta\delta_{\tilde{\ell}} q - q\tilde{\mu}), \quad (64)$$

with $\Delta\delta_{\tilde{\ell}} \in \{\Delta\delta_{a,\min}, \Delta\delta_{a,\max}\}$.

APPENDIX B

COMPLETE DERIVATIONS OF $\mathbb{E}_{\hat{\xi}_1}$ AND $\mathbb{E}_{\hat{\xi}_2}$

The general expression of $\mathbb{E}_{\hat{\xi}_1}$ in (42) and $\mathbb{E}_{\hat{\xi}_2}$ in (48) can be defined as

$$\mathbb{E}_{\hat{\xi}} \triangleq \mathbb{E}[e^{j2\pi/\lambda\{\mathcal{M}d \cos \hat{\phi}_k + \mathcal{N}d \sin \hat{\phi}_k\} \sin \hat{\theta}_k}], \quad (65)$$

where $\mathcal{M} \in \{m - \tilde{m}, m_1 + m_2 - \tilde{m}_1 - \tilde{m}_2\}$ and $\mathcal{N} \in \{n - \tilde{n}, n_1 + n_2 - \tilde{n}_1 - \tilde{n}_2\}$. $\mathbb{E}_{\hat{\xi}}$ can be calculated

using $\mathbb{E}_{\hat{\xi}} = \int_0^{2\pi} \varpi_1 f(\hat{\phi}_k) d\hat{\phi}_k$, where ϖ_1 refers to the inner integral, which is

$$\varpi_1 = \int_0^{\pi} e^{j2\pi/\lambda\{\mathcal{M}d \cos \hat{\phi}_k + \mathcal{N}d \sin \hat{\phi}_k\} \sin \hat{\theta}_k} f(\hat{\theta}_k) d\hat{\theta}_k, \quad (66)$$

where $f(\hat{\phi}_k)$ and $f(\hat{\theta}_k)$ refer to the PDF of $\hat{\phi}_k$ and $\hat{\theta}_k$, respectively, which can be expressed as $f(\hat{\phi}_k) = (1/(\sqrt{2\pi}\sigma_\phi))e^{-\frac{1}{2}(\frac{\hat{\phi}_k - \phi_k}{\sigma_\phi})^2}$ and $f(\hat{\theta}_k) = (1/(\sqrt{2\pi}\sigma_\theta))e^{-\frac{1}{2}(\frac{\hat{\theta}_k - \theta_k}{\sigma_\theta})^2}$, respectively, where σ_ϕ and σ_θ represent the variance of $\hat{\phi}_k$ and $\hat{\theta}_k$, respectively. It is worth noting that the means of $\hat{\phi}_k$ and $\hat{\theta}_k$ are ϕ_k and θ_k , respectively, since the localisation algorithms employed in this paper are unbiased.

By substituting the PDF of $\hat{\theta}_k$ in (66) and performing some algebraic manipulations, ϖ_1 can be written as

$$\varpi_1 = \int_0^\pi C_1 e^{j\nu_{\hat{\phi}} \sin \hat{\theta}_k - C_2 (\hat{\theta}_k - \theta_k)^2} d\hat{\theta}_k, \quad (67)$$

where $C_1 = 1/(\sqrt{2\pi}\sigma_\theta)$, $C_2 = 1/(2\sigma_\theta^2)$ and $\nu_{\hat{\phi}} = 2\pi/\lambda\{\mathcal{M}d \cos \hat{\phi}_k + \mathcal{N}d \sin \hat{\phi}_k\}$. However, a closed-form solution for ϖ_1 is not feasible, and thus the first item of the Taylor series of $\sin \hat{\theta}_k$ at θ_k , which is $\sin \hat{\theta}_k = \sin(\theta_k + \Delta\theta_k) \approx \sin \theta_k$, is employed to approximate $\sin \hat{\theta}_k$. Nevertheless, this sort of approximation is very accurate since the estimation errors in θ_k are small and distributed around zero with a variance drastically decreased as SNR increases. Accordingly, by substituting $\sin \hat{\theta}_k \approx \sin \theta_k$ into (67), the value of ϖ_1 is approximated as

$$\varpi_1 \approx C_1 e^{j\nu_{\hat{\phi}} \sin \theta_k} \int_0^\pi e^{-C_2 (\hat{\theta}_k - \theta_k)^2} d\hat{\theta}_k, \quad (68)$$

which, by using [41, Eq.1, pp. 108], can be found as

$$\varpi_1 \approx C_1 \sqrt{\pi/4C_2} C_3 e^{j\nu_{\hat{\phi}} \sin \theta_k}, \quad (69)$$

where $C_3 = \left\{ \text{erf}(\sqrt{C_2}(\pi - \theta_k)) - \text{erf}(\sqrt{C_2}(-\theta_k)) \right\}$.

Afterwards, by substituting the value of ϖ_1 in $\mathbb{E}_\xi = \int_0^{2\pi} \varpi_1 f(\hat{\phi}_k) d\hat{\phi}_k$, \mathbb{E}_ξ can be evaluated as

$$\mathbb{E}_\xi = \int_0^{2\pi} C_1 \sqrt{\pi/4C_2} C_3 C_4 e^{j\nu_{\hat{\phi}} \sin \theta_k - C_5 (\hat{\phi}_k - \phi_k)^2} d\hat{\phi}_k, \quad (70)$$

where $C_4 = 1/(\sqrt{2\pi}\sigma_\phi)$, $C_5 = 1/(2\sigma_\phi^2)$. However, directly calculating the integral in (70) is not feasible,

and thus the first term of the Taylor series of $\sin \hat{\phi}_k$ at ϕ_k , which is $\sin \hat{\phi}_k = \sin(\Delta\phi_k + \phi_k) \approx \sin \theta_k$, is employed to approximate $\sin \hat{\theta}_k$. In addition, the second-order Taylor expansion of $\cos \hat{\phi}_k$ at ϕ_k are employed to approximate $\cos \hat{\phi}_k$ as

$$\cos \hat{\phi}_k \approx \cos \phi_k - \sin \phi_k (\hat{\phi}_k - \phi_k) - 0.5 \cos \phi_k (\hat{\phi}_k - \phi_k)^2. \quad (71)$$

By substituting the Taylor expansions of $\sin \hat{\phi}_k$ and $\cos \hat{\phi}_k$ in $\nu_{\hat{\phi}}$, the approximated value of $\mathbb{E}_{\hat{\xi}}$ can be obtained as

$$\tilde{\mathbb{E}}_{\hat{\xi}} = C_6 \int_0^{2\pi} e^{j\tilde{\nu}_{\phi} \sin \theta_k (\hat{\phi}_k - \phi_k) - (\frac{j\nu_{\phi}}{2} \sin \theta_k + C_5)(\hat{\phi}_k - \phi_k)^2} d\hat{\phi}_k, \quad (72)$$

where $\nu_{\phi} = 2\pi \mathcal{M}d \cos \phi_k / \lambda$, $\tilde{\nu}_{\phi} = -2\pi \mathcal{M}d \sin \phi_k / \lambda$ and $C_6 = C_1 \sqrt{\pi/4} C_2 C_3 C_4 e^{j\nu_{\phi} \sin \theta_k}$.

By utilising the substitution method in integral calculations and then utilising [41, Eq.1, pp. 108], $\tilde{\mathbb{E}}_{\hat{\xi}}$ can be derived as

$$\tilde{\mathbb{E}}_{\hat{\xi}} = \frac{\sqrt{\pi}(\Xi_1 - \Xi_2)C_6 e^{-\frac{\tilde{\nu}_{\phi}^2 \sin^2 \theta_k}{4(\frac{j\nu_{\phi}}{2} \sin \theta_k + C_5)}}}{2\sqrt{\frac{j\nu_{\phi}}{2} \sin \theta_k + C_5}}, \quad (73)$$

where $\Xi_p \forall p \in \{1, 2\}$ is given by

$$\Xi_p = \operatorname{erf} \left(\frac{2(\phi_k - 2\pi(p-1))(\frac{j\nu_{\phi}}{2} \sin \theta_k + C_5) + j\tilde{\nu}_{\phi} \sin \theta_k}{2\sqrt{\frac{j\nu_{\phi}}{2} \sin \theta_k + C_5}} \right). \quad (74)$$

REFERENCES

- [1] M. Al-Jarrah, M. A. Yaseen, A. Al-Dweik, O. A. Dobre, and E. Alsusa, "Decision fusion for IoT-based wireless sensor networks," *IEEE IoT J.*, vol. 7, no. 2, pp. 1313-1326, 2020.
- [2] Z. Lyu, G. Zhu and J. Xu, "Joint maneuver and beamforming design for UAV-enabled integrated sensing and communication," *IEEE Trans. Wireless Commun.*, 2022.
- [3] M. Al-Jarrah, A. Al-Dweik, E. Alsusa, and E. Damiani, "RFID reader localization using hard decisions with error concealment," *IEEE Sens. J.*, vol. 19, no. 17, pp. 7534-7542, 2019.
- [4] T. Wang, F. Fang and Z. Ding, "An SCA and relaxation based energy efficiency optimization for multi-user RIS-assisted NOMA networks," *IEEE Trans. Veh. Technol.*, vol. 71, no. 6, pp. 6843-6847, Jun. 2022.
- [5] T. Wang, F. Fang and Z. Ding, "Joint phase shift and beamforming design in a multi-user MISO STAR-RIS assisted downlink NOMA network," *IEEE Trans. Veh. Technol.*, vol. 72, no. 7, pp. 9031-9043, July 2023.
- [6] Z. Xu and A. Petropulu, "A bandwidth efficient dual-function radar communication system based on a MIMO radar using OFDM waveforms," *IEEE Trans. Signal Process.*, vol. 71, pp. 401-416, 2023.

- [7] J. Steinwandt, F. Roemer, M. Haardt, and G. D. Galdo, "Performance analysis of multi-dimensional ESPRIT-type algorithms for arbitrary and strictly non-circular sources with spatial smoothing," *IEEE Trans. Signal Process.*, vol. 65, no. 9, pp. 2262-2276, May 2017.
- [8] X. Zhang *et al.*, "Localization of near-field sources: A reduced-dimension MUSIC algorithm," *IEEE Commun. Lett.*, vol. 22, no. 7, pp. 1422-1425, Jul. 2018.
- [9] B. Tang, *et al.*, "Maximum likelihood estimation of DOD and DOA for bistatic MIMO radar," *Signal Process.*, vol. 93, no. 5, pp. 1349-1357, May 2013.
- [10] Q. Zhang, *et al.*, "Power scaling of uplink massive MIMO systems with arbitrary-rank channel means," *IEEE J. Sel. Topics Signal Process.*, vol. 8, no. 5, pp. 966-981, Oct. 2014.
- [11] J. Wang, *et al.*, "First demonstration of joint wireless communication and high-resolution SAR imaging using airborne MIMO radar system," *IEEE Trans. Geosci. Remote Sens.*, vol. 57, no. 9, pp. 6619-6632, Sep. 2019.
- [12] F. Liu, *et al.*, "Toward dual-functional radar-communication systems: Optimal waveform design," *IEEE Trans. Signal Process.*, vol. 66, no. 16, pp. 4264-4279, Aug. 2018.
- [13] Z. Du, *et al.*, "Integrated sensing and communications for V2I networks: Dynamic predictive beamforming for extended vehicle targets," *IEEE Trans. Wireless Commun.*, vol. 22, no. 6, pp. 3612-3627, Jun. 2023.
- [14] C. Ouyang, Y. Liu and H. Yang, "Performance of downlink and uplink integrated sensing and communications (ISAC) systems," *IEEE Wireless Commun. Lett.*, vol. 11, no. 9, pp. 1850-1854, Sep. 2022.
- [15] C. Ouyang, Y. Liu, and H. Yang, "MIMO-ISAC: Performance analysis and rate region characterization," *IEEE Wireless Commun. Lett.*, 2023.
- [16] M. Al-Jarrah, E. Alsusa and C. Masouros, "A unified performance framework for integrated sensing-communications based on KL-divergence," *IEEE Trans. Wireless Commun.*, doi: 10.1109/TWC.2023.3270390.
- [17] M. Al-Jarrah, E. Alsusa and C. Masouros, "Kullback-Leibler divergence analysis for integrated radar and communications (RadCom)," *2023 IEEE Wireless Commun. and Netw. Conf. (WCNC)*, Glasgow, UK, 2023.
- [18] X. Wang, Z. Fei and Q. Wu, "Integrated sensing and communication for RIS-assisted backscatter systems," *IEEE IoT J.*, vol. 10, no. 15, pp. 13716-13726, Aug. 2023.
- [19] X. Wang, *et al.*, "Joint waveform and discrete phase shift design for RIS-assisted integrated sensing and communication system under Cramer-Rao bound constraint," *IEEE Trans. Veh. Technol.*, vol. 71, no. 1, pp. 1004-1009, Jan. 2022.
- [20] S. Han, M. A. Al-Jarrah and E. Alsusa, "Performance evaluation of MIMO radars under a generalized model of array imperfections," *IEEE Trans. Aerosp. Electron. Syst.*, doi: 10.1109/TAES.2023.3304617.
- [21] S. Han, M. Al-Jarrah and E. Alsusa, "Joint DOA and Doppler frequency estimation for MIMO radars in the presence of array model imperfections," *2023 IEEE Wireless Commun. and Netw. Conf. (WCNC)*, Glasgow, UK, 2023.
- [22] S. Han, M. Al-Jarrah and E. Alsusa, "Efficient localization algorithms using a uniform rectangular array with model imperfections," *2023 IEEE Wireless Commun. and Netw. Conf. (WCNC)*, Glasgow, UK, 2023.
- [23] Z. Dai, W. Su and H. Gu, "A Gain and phase autocalibration approach for large-scale planar antenna arrays," *IEEE Commun. Lett.*, vol. 25, no. 5, pp. 1645-1649, May 2021.
- [24] S. Song, X. Ma, W. Sheng and R. Zhang, "Maximum likelihood sensor array calibration using non-approximate Hessian matrix," *IEEE Signal Process. Lett.*, vol. 28, pp. 688-692, 2021.
- [25] M. Wang, Z. Zhang, and A. Nehorai, "Performance analysis of coarray-based MUSIC in the presence of sensor location errors," *IEEE*

- Trans. Signal Process.*, vol. 66, no. 12, pp. 3074-3085, Jun. 2018.
- [26] P. Chen, Z. Chen, Z. Cao, and X. Wang, "A new atomic norm for DOA estimation with gain-phase errors," *IEEE Trans. Signal Process.*, vol. 68, pp. 4293-4306, 2020.
- [27] Y. Guo, X. Hu, W. Feng, and J. Gong, "Low-complexity 2D DOA estimation and self-calibration for uniform rectangle array with gain-phase error," *Remote Sens.*, vol. 24, no. 9, pp. 1303-1307, Sept. 2017.
- [28] B. Liao and S. -C. Chan, "Direction-of-Arrival estimation in subarrays-based linear sparse arrays with gain/phase uncertainties," *IEEE Trans. Aerosp. Electron. Syst.*, vol. 49, no. 4, pp. 2268-2280, Oct. 2013.
- [29] Z. Yang *et al.*, "Sparsity-based STAP using alternating direction method with gain/phase errors," *IEEE Trans. Aerosp. Electron. Syst.*, vol. 53, no. 6, pp. 2756-2768, 2017.
- [30] W. Liu *et al.*, "Design a novel target to improve positioning accuracy of autonomous vehicular navigation system in GPS denied environments," *IEEE Trans. Ind. Informat.*, vol. 17, no. 11, pp. 7575-7588, Nov. 2021
- [31] S. Misra *et al.*, "Cooperative localization of a GPS-denied UAV using direction-of-arrival measurements," *IEEE Trans. Aerosp. Electron. Syst.*, vol. 56, no. 3, pp. 1966-1978, Jun. 2020.
- [32] X. Qian, M. Di Renzo and A. Eckford, "K-means clustering-aided non-coherent detection for molecular communications," *IEEE Trans. Commun.*, vol. 69, no. 8, pp. 5456-5470, Aug. 2021.
- [33] Z. Gao *et al.*, "Integrated sensing and communication with mmWave massive MIMO: A compressed sampling perspective," *IEEE Trans. Wireless Commun.*, 2022.
- [34] M. Jana *et al.*, "Pre-equalized faster-than-Nyquist transmission," *IEEE Trans. Commun.*, vol. 65, no. 10, pp. 4406-4418, Oct. 2017.
- [35] P. Heidenreich, A. M. Zoubir and M. Rubsamen, "Joint 2-D DOA estimation and phase calibration for uniform rectangular arrays," *IEEE Trans. Signal Process.*, vol. 60, no. 9, pp. 4683-4693, Sep. 2012.
- [36] M. A. Al-Jarrah *et al.*, "Error rate analysis of amplitude-coherent detection over Rician fading channels with receiver diversity," *IEEE Trans. Wireless Commun.*, vol. 19, no. 1, pp. 134-147, Jan. 2020.
- [37] A. van den Bos, "The multivariate complex normal distribution-a generalization," *IEEE Trans. Inf. Theory*, vol. 41, no. 2, pp. 537-539, Mar. 1995.
- [38] Y. Li and M. H. Er, "Theoretical analyses of gain and phase error calibration with optimal implementation for linear equispaced array," *IEEE Trans. Signal Process.*, vol. 54, no. 2, pp. 712-723, Feb. 2006.
- [39] P. Stoica and R. L. Moses, *Spectral analysis of signals*. Upper Saddle River, NJ, USA: Prentice-Hall, 2005.
- [40] J. Pan, C. Zhou, B. Liu, and K. Jiang, "Joint DOA and Doppler frequency estimation for coprime arrays and samplers based on continuous compressed sensing," *2016 CIE Int. Conf. Radar (RADAR)*, pp. 1-5, 2016.
- [41] I. S. Gradshteyn and I. M. Ryzhik, *Tables of integrals, series and products*. 7th ed. Oxford: Academic, 2007.